Global Influences on the Indian Monsoon: Testing Existing Hypotheses with Climate Indices

Madison G. Shankle[1]

Advisers: Ronald B. Smith[1]*, Caroline C. Ummenhofer*[2]

Second Reader: Alexey V. Fedorov[1]

[1] Department of Geology & Geophysics, Yale University

[2] Department of Physical Oceanography, Woods Hole Oceanographic Institution

A Senior Thesis presented to the faculty of the Department of Geology and Geophysics, Yale University, in partial fulfillment of the Bachelor's Degree.

Abstract

This study investigates postulated relationships between the Indian monsoon and the global-scale climate phenomena of the El Niño Southern Oscillation (ENSO), global warming, and the Indian Ocean Dipole (IOD). Climate indices are used to track monthly and interannual variations in different features of these climate phenomena, and statistical correlation of these indices (calculated from the NCEP Reanalysis-2 dataset) is interpreted to inform potential relationships between the monsoon and the various climate phenomena of interest. The results found herein not only demonstrate the indices' capacity to capture important climatic events and variations; it also reveals certain correlative relationships between the Indian monsoon and the other climate phenomena mentioned. First, the monsoon and ENSO appear to be better correlated (higher correlation coefficients between more indices) in their interannual variations (JJA averages of indices) than in their seasonal or monthly variations (monthly values of indices). The opposite is true of the monsoon and global warming and the monsoon and the IOD. Secondly, ENSO appears more well correlated with dynamic atmospheric indices of the Indian monsoon, such as zonal vertical wind shear and velocity potential at 850hPa, rather than thermodynamic moisture-related indices, such as total rainfall, moisture flux, or moist static energy. No such pattern is discernable with the global warming or IOD indices. Finally, skewness and kurtosis values of the various indices' distributions reveal interesting patterns in the bimodality of certain indices. While many indices exhibit bimodality in the distribution of their monthly values across the dataset, some indices retain this bimodality in their interannual values (JJA averages). We speculate that such indices exhibit bimodality across their monthly values simply as an overprint of the strong bimodality of their primary forcing (namely the seasonal cycle of solar insolation); however, their retention of some bimodality in their interannual distributions (across JJA values) suggests some degree of bimodality being inherent to their internal systems, separate from the bimodality of their forcing. While being far from able to inform any causation between the relationships observed here, this study represents a robust attempt to quantify and demonstrate postulated relationships between climate phenomenon that are conventionally only accepted based on physical theory. The indices both capture historically accepted relationships between climate phenomena as well as hint at new ones, making an important first step towards characterizing these complex climatic processes in a compartmentalized and systematic manner.

Table of Contents

1. Introduction

This study makes a thorough and systematic investigation of postulated relationships between the Indian monsoon and a number of global-scale climate phenomena, namely the El Niño Southern Oscillation (ENSO), global warming, and the Indian Ocean Dipole (IOD). The methodology of

this study is based exclusively on the use of pre-defined indices meant to indicate the presence or magnitude of a climatic event or process. Such indices provide a means of quantifying climatic phenomenon that is both intuitive and objective, and the robustness of the results here in part justifies their use in climate studies. We therefore investigate relationships between the Indian monsoon and other climate phenomenon through statistical correlation of these indices. This study represents an attempt to demonstrate and quantify relationships between climate phenomenon that are traditionally only accepted through theory and principles of physics. Here, we display various physical processes made visible in these indices and then go on to investigate connections between those of the Indian monsoon and different climate phenomena. All indices are calculated from the NCEP Reanalysis V2 dataset (see Appendix section A1. The Reanalysis Dataset).

2. Background – What Phenomena Impact the Indian Monsoon?

2.1. El Niño Southern Oscillation (ENSO)

Almost one hundred years ago, Sir Gilbert Walker perceived the connection between the Southern Oscillation and Indian summer monsoon. Since then, numerous studies have evinced the relationship between the El Niño-Southern Oscillation (ENSO) and the Indian monsoon (cited in Torrence and Webster, 1999: Walker and Bliss 1937; Shukla and Paolino 1983; Joseph et al, 1994). The conventional description of ENSO-induced teleconnection response in the monsoon is through the large-scale east-west shifts in the tropical Walker circulation (Kumar et al, 1999). During an El Niño (warm) event, a warming of sea surface temperatures (SSTs) in the central and eastern Pacific is accompanied by diminished easterly trade winds and an eastward shift the ascending limb of the Walker circulation. Consequently, there is anomalous subsidence that extends form the western Pacific to the Indian subcontinent, suppressing convection and precipitation there and acting to weaken the Indian monsoon. Conversely, a La Niña (cold) event produces anomalously cool SSTs in the central and eastern Pacific, shifting warm SSTs and convection westward and enhancing easterly trades (cited in Torrence and Webster, 1999: Rasumusson and Carpenter 1982). In this scenario, the Walker circulation is dominated by a

strong, anomalous east-west cell with descending motion in the eastern Pacific and is accompanied by enhanced monsoon precipitation (Figure 1) (Krishnamurthy and Goswami, 2000).

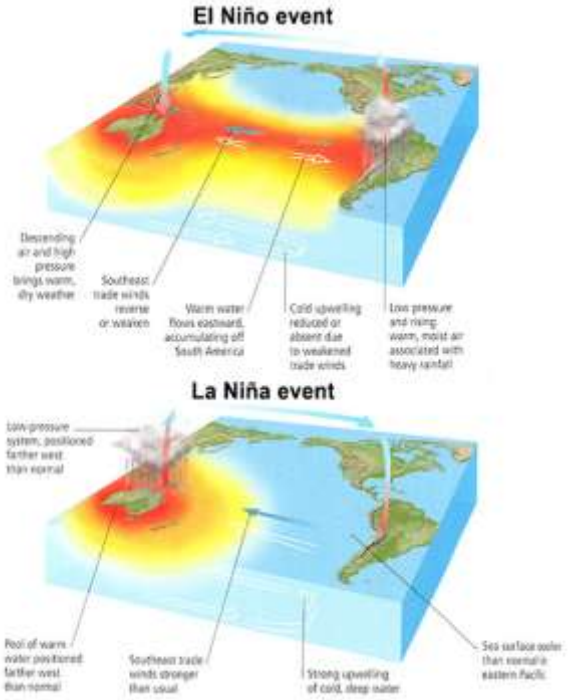

Figure 1: Illustration of the defining features of El Niño and La Niña events, namely SST, pressure, and circulation anomalies.. Mann & Kump, Dire Predictions: Understanding Climate Change, 2nd Edition

The historical record (~140 years) shows this inverse relationship between ENSO and the Indian monsoon (weak monsoon precipitation in years of warm/El Niño events and strong monsoon precipitation in years of cold/La Niña events) (Kumar et al, 1999; cited in Krishnamurthy and Goswami, 2000: Sikka 1980; Pant and Parthasarathy 1981; Rasmusson and Carpenter 1983; Shukla and Paolino 1983; Parthasarathy and Pant 1985; Shukla 1987). The long-term (127-year) correlation between seasonal anomalies of IMR and Niño-3 SST (an index for ENSO) is -0.63 and significant at the 99.9% level. This inverse correlation is displayed in Figure 2 and represents the tendency of the Indian monsoon to be below normal in warm El Niño events and above normal in cold La Niña events. This relationship is not always perfect, however, and it is apparent that the interannual variability of this ENSO-monsoon relationship changes in an

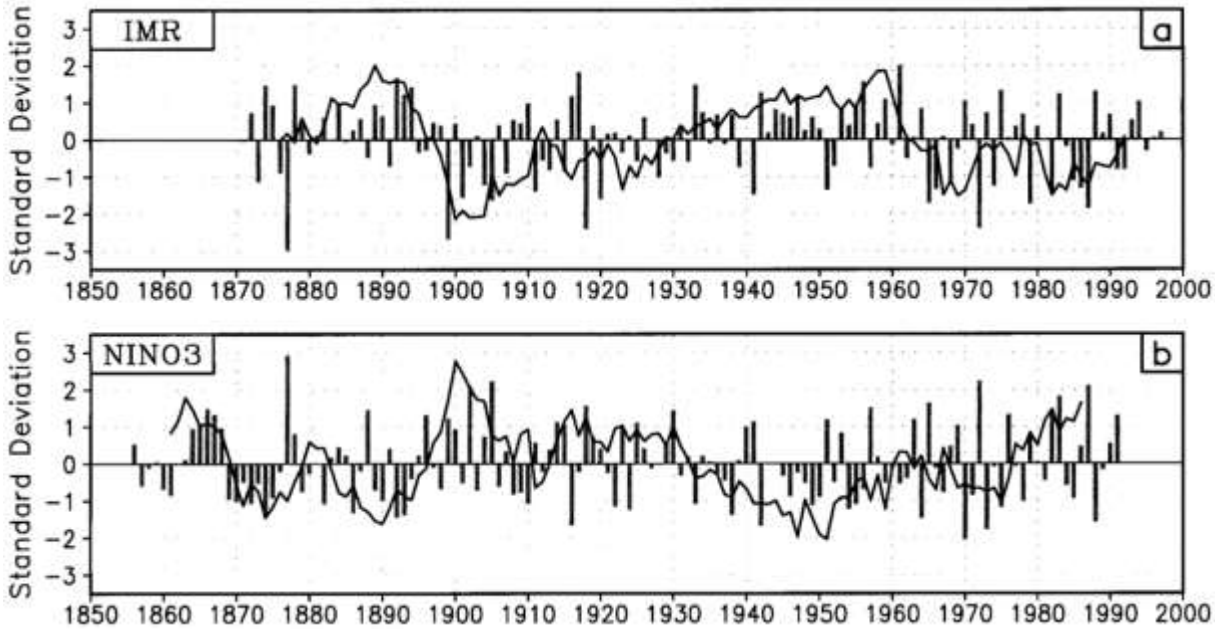

Figure 2. (a) Time series of JJAS seasonal anomaly of IMR (bar) and its 11-yr running mean (solid line). (b) Same as (a) but for JJAS seasonal anomaly of Niño-3 SST. The time series are plotted in their corresponding standard deviation units. The interannual standard deviation of IMR is 0.66 mm day^{-1} while the interdecadal standard deviation is 0.2 mm day^{-1}. For Niño-3, the standard deviations of interannual and interdecadal variation s are 0.67 K and 0.15 K, respectively. Taken from Krishnamurthy and Goswami, 2000.

interdecadal mode.

2.2. Global Warming

The effects of global warming on the Indian monsoon could be diverse. Warmer ocean temperatures are expected to evaporate more water vapor into the air above it, increasing moisture fluxes onto the Indian subcontinent by nature of the increased quantity of water vapor in the air. Beyond this, warmer air (being warmed from these elevated SSTs and/or global warming generally) is also expected to have an increased capacity to hold moisture by the Clausius-Clapeyron relation. The Clausius-Clapeyron relation states that the vapor pressure of any substance increases with temperature. The implication of this important physical concept is that, as a warmer ocean warms the air immediately above it, that air should, in the absence of other effects, be able to hold approximately 7% more water vapor for every kelvin of warming it experiences [Allan and Soden, 2008; Wentz et al., 2007]. Elevated SSTs could thus positively contribute to moisture transport and extreme precipitation events in the future. Finally, warm SSTs are known to be conducive to convective circulation; Taschetto et al. (2010) demonstrate 28^{o}C being an approximate threshold temperature that tends to induce deep, heavy-precipitation-generating convection.

Additionally, increasing land surface temperatures, which are expect to rise more rapidly than sea surface temperatures, could increase the land-sea temperature gradient, which would be expected to increase precipitation by way of strengthening onshore winds bring moisture onto the subcontinent. The seasonal reversal of winds in the summer months onto the subcontinent is believed to be driven by this strong land-sea surface temperature gradient that develops in India in the summer months. In summer months, the accelerated warming of the India's land surface over its surrounding oceans generates a low-pressure center in the atmosphere, inducing a strong southwesterly flow as winds converge toward this low. There has been some debate recently about this model of the ISM, however. While the classical land-sea surface temperature gradient adequately explains the seasonal reversal of surface winds, Goswami and Chakravorty (2017) discuss how it fails to explain both the onset and deep vertical extent of ISM circulation. They argue that the surface temperature over land cools after monsoon onset and is therefore insufficient to maintain the monsoon throughout its whole season; instead they explain that it is the tropospheric temperature gradient that becomes and remains positive through the monsoon season. It is this change in sign of the tropospheric temperature gradient that leads to the northward progression of the Intertropical Convergence Zone (ITCZ) and its precipitation,

initiating and sustaining the ISM (Goswami and Chakravorty, 2017). If this model is correct, then this effect of enhanced land surface temperatures with global warming might be irrelevant. Where the current literature stands, however, the Indian monsoon is driven to a first order by a stark contrast between warm land temperatures and cool ocean temperatures in the summer, and so this effect of global warming, both land- and ocean-based, will be investigated in this study.

2.3. Indian Ocean Dipole (IOD)

The Indian Ocean Dipole (IOD) is a system of internal variability within the Indian Ocean characterized by oscillating SSTs patterns in the eastern and western Indian Ocean, analogous in some ways to ENSO. These SST anomalies are associated with changes to wind speed and direction as well as precipitation (Anil et al., 2016). Saji et al. (1999) first described the correlation between the IOD and the Indian monsoon and showed the IOD to be independent of ENSO. During a positive phase of the IOD, westerly winds along the equator weaken, allowing warm water of the Pacific Warm Pool to shift towards Africa in the west and cool water to rise up from the deep ocean in the east. This sets up a positive temperature gradient going from east to west across the Indian Ocean, accompanied by enhanced convection and rainfall over the Arabian Sea, which subsequently gets blown onto the Indian subcontinent, enhancing the monsoon (Figure 3, top). Conversely, during a negative IOD phase, westerly winds intensify along the equator, concentrating warm waters near Indonesia. The temperature gradient now increases going west to east, and convective activity is concentrated over the eastern Indian Ocean, away from the landmass of India. This is interpreted to weaken monsoon intensity in that year (Figure 3, bottom). (Saji et al., 1999).

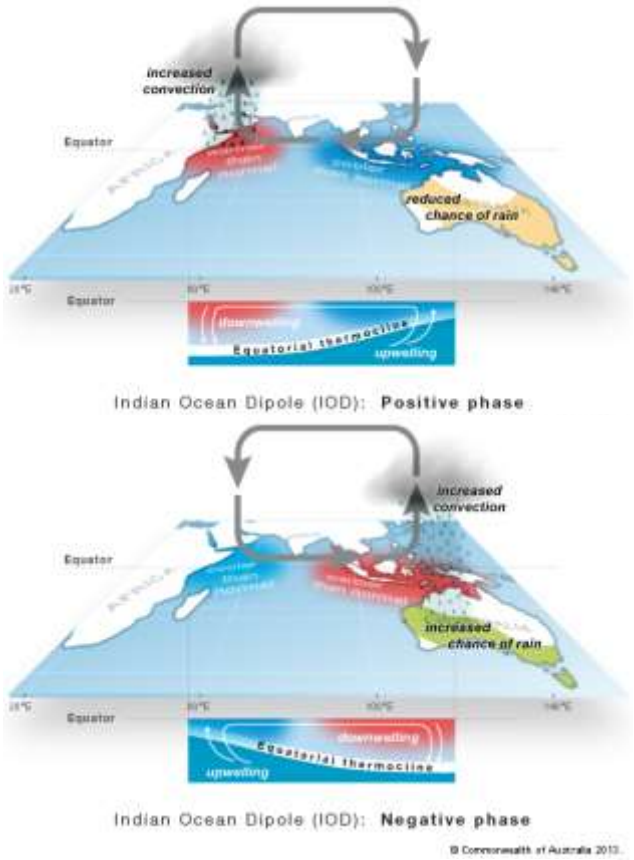

Figure 3: An illustration of the deining features of positive (top) and negative (bottom) phases of the IOD. Australia Bureau of Meteorology, http://www.bom.gov.au/climate/iod/.

3. Methods

The methodology of this study is based exclusively on the use of climatic indices. We define an index as a calculated or averaged value of a variable(s) designed to indicate the onset or intensity of a climate phenomenon. Some indices are well-accepted and

widely used, especially around ENSO (e.g. the Niño-3.4 SST index and the Southern Oscillation Index (SOI)). The majority of our climate indices are garnered from the bodies of literature around the respective climate phenomena, but we do define a extra monsoon indices on the basis of basic physical and meteorological principles (these are discussed in section 4).

We calculate our indices from the National Center for Atmospheric Research (NCAR) project, NCEP/DOE Reanalysis-2, by the NOAA/OAR/ESRL PSD, Boulder, Colorado, USA (web site at https://www.esrl.noaa.gov/psd/). This is a global reanalysis of atmospheric and oceanic data spanning 1982 to 2016, although some variables are now available up through 2018. This reanalysis represents an improvement to the Reanalysis-1 project by incorporating satellite-based observations into the previous matrix of surface, air-balloon, and aircraft observations of such variables as sea surface temperature and land surface temperature. The data consist of a global grid at a 2.5-degree by 2.5-degree horizontal resolution with 17 standard pressure levels ranging from 1000 to 100hPa in the vertical. As for temporal resolution, the data is available as 6-hour, daily, and monthly products. (Kanamitsu et al., 2002; Kalnay et al., 1996).

This data was processed, indices calculated, and results plotted all within NCL (NCAR Command Language) version 6.4.0. NCL is a free interpreted language designed specifically for climate data processing and visualization, being compatible with a wide range of file formats specific to climate data. Some of the unique features of NCL over other coding languages are its incorporation of metadata with its variables, its ability to import data of a variety of formats, and a scheme that supports array-based functions, all of which make it ideal for handling climatic variables ("The NCAR Command Language (Version 6.4.0)", http://dx.doi.org/10.5065/D6WD#XH5).

4. The Indices

The methodology of this study is based exclusively on the use of climatic indices. These indices are calculated quantities or averages of various climatic variables meant to indicate the onset or intensity of the monsoon, ENSO, global warming, or the IOD. The beauty of such indices – if they are soundly based on meteorological and physical theory – is that they should capture fundamental patterns and reduce noisy, complex, or multifaceted climatic phenomena into intuitive and easily quantifiable data. Various indices have been taken from the literature as well as the National Oceanic and Atmospheric Administration (NOAA) and National Aeronautics and Space Administration (NASA) to represent the onset and magnitudes of the climate phenomena

discussed here. The nature and significance of the indices are summarized in Table 1; most of the indices' areal extents are displayed in Figure 12. This paper will describe these climatic indices and the physics behind them before going on to investigate their robustness in capturing important climate phenomena. then, correlations between these indices will be used to evince any relationships between the indian monsoon and enso, global warming, and/or the iod.

4.1. Seasonality Index – Incoming Solar Radiation (solar_rad)

Incoming solar radiation is, to a first-order, the primary driver of the monsoon. As a result of its seasonal intensification over India every summer, the land surface of the Indian subcontinent warms rapidly relative to Indian Ocean (which has a high heat capacity and thus large thermal inertial), creating a pressure low over the subcontinent which induces warm, moisture-laden winds to blow onto the land off of the India Ocean and especially the Arabian Sea with the seasonal reversal of zonal winds (Goswami and Chakravorty, 2017). We include incoming solar radiation as an index in our study to serve as a proxy for the seasonal cycle. Being a factor exclusively of the obliquity and eccentricity of the Earth's tilt (Milankovitch Cycles, varying on the order of tens to hundreds of years), it cyclicity every year is virtually constant year after year in our dataset. More importantly, it represents the external forcing common to the rest of the other indices. We include it so that we can assess the confounding role seasonality might play in correlation between the various climate indices.

4.2. Monsoon Indices

4.2.1. Extended Indian Monsoon Rainfall (precip_EIMR)

Historically, monsoon strength has most commonly been characterized in terms of an area-averaged quantity of precipitation, averaged either monthly or across the June-July-August (JJA) season (Shukla and Mooley, 1987). The Indian Monsoon Rainfall (IMR) index is one such conventional, precipitation-based measure of monsoon strength. IMR is defined as the weighted average of rainfall observed at 306 well-distributed rain gauge stations over India (Parthasarathy et al., 1992). However, this index was shown to have a low correlation with other monsoon indices – especially the zonal wind-shear between 850 and 200hPa – by Goswami et al. (1999), who developed a new index that they named the Extended Indian Monsoon Index (EIMR). The EIMR is defined as the total precipitation averaged over 70-110E and 10-30N (referred to as the "EIMR" region, Figure 4) and improves upon the old IMR index by accounting for the large annual amounts of precipitation falling over the Bay of Bengal, which the group demonstrates to

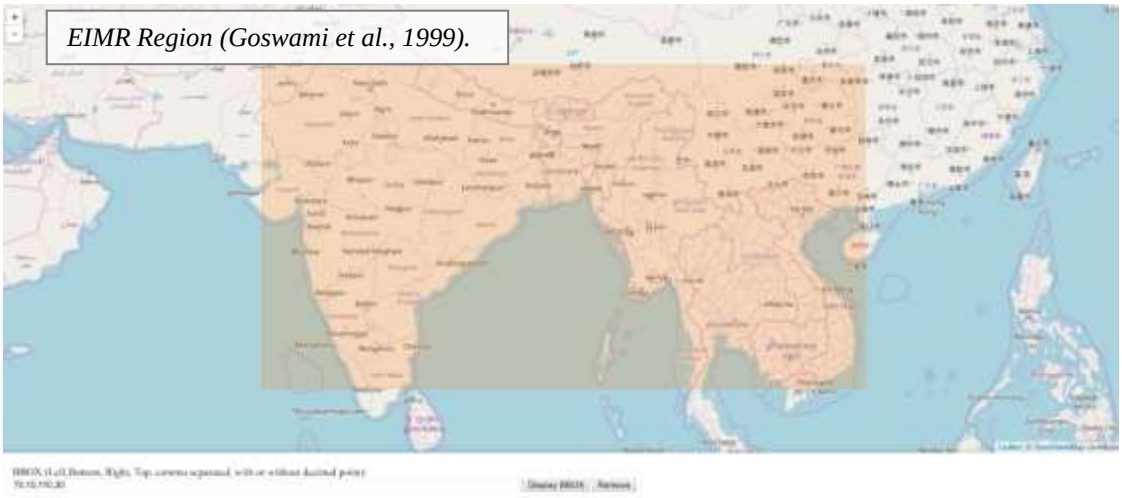

Figure 4: Region of the Extended Indian Monsoon Rainfall (EIMR) region as defined by Goswami et al. (1999): 10-

have significant relevance to the Indian monsoon. Goswami et al. (1999) further assert that the EIMR index is superior to the IMR index for its ability to better represent variability in total monsoon convective heating, which the IMR index, being based primarily on rain-gauge data over the Indian continent, cannot account for. Given that the monsoon is, to a first-order, a baroclinic response to diabatic heating over the south Asian region, it is imperative that any monsoon index correlate well with this heating in addition to monsoon precipitation (Goswami et al., 1999). The traditional IMR index has very low correlation with diabetic heating-related indices such as zonal wind shear, which is why we choose to investigate the EIMR index as an indicator of monsoon strength in this study.

4.2.2. Zonal Vertical Shear (vert_shear_u)

While precipitation-based monsoon indices hold the advantage of being intuitive, precipitation itself is arguably one of the noisier and more difficult climate variables to interpret and is additionally plagued by problems of poor continuity and accuracy in historical records. Webster and Yang (1992) were among the first to identify an alternative indicator of monsoon activity based on atmospheric circulation dynamics. From circulation statistics compiled and archived at a number of meteorological centers throughout the globe, Webster and Yang (1992) demonstrated the relevance of an index based on the magnitude of the mean summer vertical shear in the South Asia region. Their justification for such an index was heavily supported by physical theories of monsoon dynamics. To a first-order, the monsoon circulation is largely a low-frequency baroclinic Rossby-wave response to seasonal continental heating. In late boreal spring, with the development of increasingly warmer land temperatures over the Indian subcontinent and an associated pressure low in the overlying atmosphere, local lower

tropospheric winds switch rapidly from weak easterlies to strong westerlies coming off the Arabian Sea, while upper tropospheric westerlies decelerate. These physics are described by the Thermal Wind Equation, which balances Coriolis and pressure-gradient forces and describes how vertical wind shear develops as a function of a meridional temperature gradient (Equation 1 where v_g is the geostrophic wind vector, P is pressure as a vertical coordinate, R is the gas constant for air, f is the Coriolis parameter, k is a vertically-directed unit vector, and ∇_P is the isobaric del operator) ("Thermal Wind Equation", American Meteorology Society Glossary of Meteorology).

$$-\frac{\partial \boldsymbol{v_g}}{\partial P} = \frac{R}{Pf}\boldsymbol{k} \times \nabla_P T \quad [1]$$

The weakening of upper-level westerly winds and intensification of those below can easily be measured by the difference in zonal winds at 850hPa and at 200hPa. Defining the zonal vertical wind shear index as

$$Vertical\ shear = u(200hPa) - u(850hPa) \quad [2]$$

will produce negative zonal wind shear values with the weakening of westerly winds aloft and strengthening of those below during the monsoon season, while returning to positive values the rest of the year. The magnitude of this reversal in winds and the negative values of this vertical shear index during the monsoon should therefore give a robust indication of the strength of the monsoon that year. Webster and Yang (1992) averaged their vertical wind shear over 40-110E, 0-20N, however we have modified this range to 10-35N, 65-95E to include less ocean surface and focus on winds above the land surface of India, where we expect thermal wind dynamics to be strongest. We use this defined area in a number of other monsoon indicators for consistency and will refer to it as the "All India" region (Figure 5).

Figure 5: "All India" region as defined by Shankle:10-35N, 65-95E for the purpose of area-averaging certain monsoon indices.

4.2.3. Velocity Potential at 200hPa and 850hPa (vp200, vp850)

Velocity potential is defined as the scalar function whose gradient is equal to the velocity vector u of an irrotational flow, as given by 3 where ∅ is the velocity

potential ("Velocity Potential", American Meteorology Society Glossary of Meteorology).

$$\boldsymbol{u} = \nabla\emptyset \quad [3]$$

Velocity potential is only associated with the irrotational component of winds, making it a powerful indicator of monsoon strength for its ability to describe the convergence or divergence in the wind flow field. Figure 6 shows how the velocity potential relates to convergence and divergence in the u vector. As the slope (gradient) of the black curve transitions from positively-sloped to negatively-sloped velocity potential across the x-space, the velocity field in this space must necessarily transition from being negatively-directed to positively-directed, opposite of the gradient of the velocity potential. This pattern represents divergence in the velocity field, as shown by the arrow annotations. The grey curve demonstrates the opposite; as the slope (gradient) of the velocity potential goes from negatively-sloped to positively-sloped, the velocity vector must go from positively-directed to negatively-directed, producing convergence. An important assumption made at this point is the sign of velocity potential co-varying inversely with that of divergence in the velocity flow field. This assumption is commonly made in areas, such as India, in which the strongest values of convergence or divergence are expected to occur in the center of your spatial domain (i.e. over the warm land mass of India relative to the surrounding ocean) with lesser values surrounding. This makes the scheme displayed in Figure 6 more probable to be realistic. In this case, positive values of velocity potential would indicate convergence (negative divergence), while negative values of velocity potential would indicate divergence.

By this logic, velocity potential is reported in climate studies as indicator of subsidence and thus is commonly accepted as a strong proxy for ascending (descending) motion associated with anomalous Walker circulation near India during El Niño (La Niña) years (Kumar et al., 2006). The use of velocity potential over other variables such as pressure and geopotential heights is further justified (a) at low latitudes, where geostrophic balance breaks down with the decreasing Coriolis

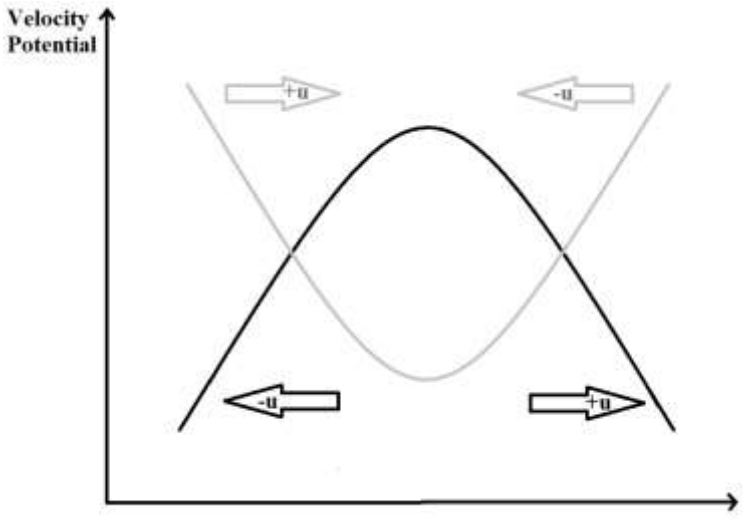

Figure 6 - Schematic meant to illustrate velocity potential's relationship to the velocity field.

parameter, and (b) for flow patterns whose spatial scales are less than the Rossby radius of deformation (Li and McWilliams, 2006).

In the context of a typical monsoon season, however, velocity potential at the 850hPa and 200hPa pressure levels is accepted as representing fundamental monsoon dynamics. At lower levels (850hPa), the monsoon exhibits positive velocity potential values over the Indian subcontinent, indicating convergence and – subsequently – the ascending motion and convection that produces monsoon rains. Monsoon dynamics then exhibit negative velocity potential values and divergence at upper levels (200hPa), where the rising air slows, loses its buoyancy, and spreads laterally. Velocity potential accurately captures these basic monsoon circulation patterns, and it is for this reason that it is taken as an indicator of monsoon strength. We again take the area-average of this variable across the "All India" region (Figure 5).

4.2.4. Mid-tropospheric Relative Humidity, 400hPa-700hPa (rhavg400700)

Moistening of the mid-troposphere by underlying convection may also serve as an indicator of monsoon onset and intensity. Parker et al. (2016) recently produced a study showing monsoon onset over South Asia being coincident with weakening of mid-level dry advection by northwesterlies over India; these findings explain the onset of the Indian monsoon in terms of a balance between the low-level monsoon flow and an overrunning intrusion of mid-tropospheric dry air. Normal mid-level (~600hPa) monsoon winds tend to be northwesterly, at an angle or perpendicular to the low-level westerly or southwesterly monsoon winds. Parker et al. (2016) demonstrate that the mid-level winds form a wedge of dry air that is deep in the northwest and shallows and over-runs the low-level monsoon winds towards the southeast. As the advection of moisture from the Arabian Sea strengthens at the onset of the monsoon, the mid-level dry air receives moisture from cumulus and congestus clouds formed below. This shallows the dry wedge through its horizontal extent, forcing the northern limit of moist convection (and thus the monsoon) to the northwest. This northwest propagation of convection marks the onset and development of the Indian monsoon and, through mid-tropospheric (~400-700hPa) relative humidity, offers a more robust alternative to the traditional, and somewhat arbitrary, definition of monsoon onset by the India Meteorological Department (IMD) – the first sustained rains over Kerala in southwest India, climatologically occurring on June 1st with a standard deviation of 8-9 days (Krishnamurthy and Shukla, 2000; Ju and Slingo, 1995). To detect the retreat of this dry wedge and the moistening of the mid-troposphere during monsoon months, we have defined a

mid-tropospheric relative humidity index as the area-averaged (over the "All India" region) relative humidity, averaged over the 400 to 700hPa pressure levels.

4.2.5. Zonal Moisture Flux Over India and the Arabian Sea (MF_Ind, MF_Arab)

As a result of the northward excursion of the ITCZ during the summer months, especially over the South China Sea and southeast Asia, typical easterlies at low levels over the Arabian Sea and India get reversed into southwesterlies (Figure 7, Goswami and Chakravorty, 2017). These southwesterly winds are important for bringing moisture-laden air into the subcontinent off of the Arabian Sea, supplying the Indian monsoon with the greater part of its moisture budget. By calculating the moisture flux as the product of specific humidity and zonal wind speed, the reversal of these winds and the resulting delivery of moisture into the Indian subcontinent can be recorded and quantified. We define two moisture flux indices, one over the Arabian Sea and one over central India, to quantify this moisture flux during the monsoon. Both are integrated over the entire atmospheric column, and they are area-averaged over an "Arabian Sea" region defined by the author (5-25N, 55-75E, Figure 8) and the "All India" region (Figure 5) previously mentioned.

4.2.6. Moist Static Energy Over India and the Arabian Sea (MSE_Ind, MSE_Arab)

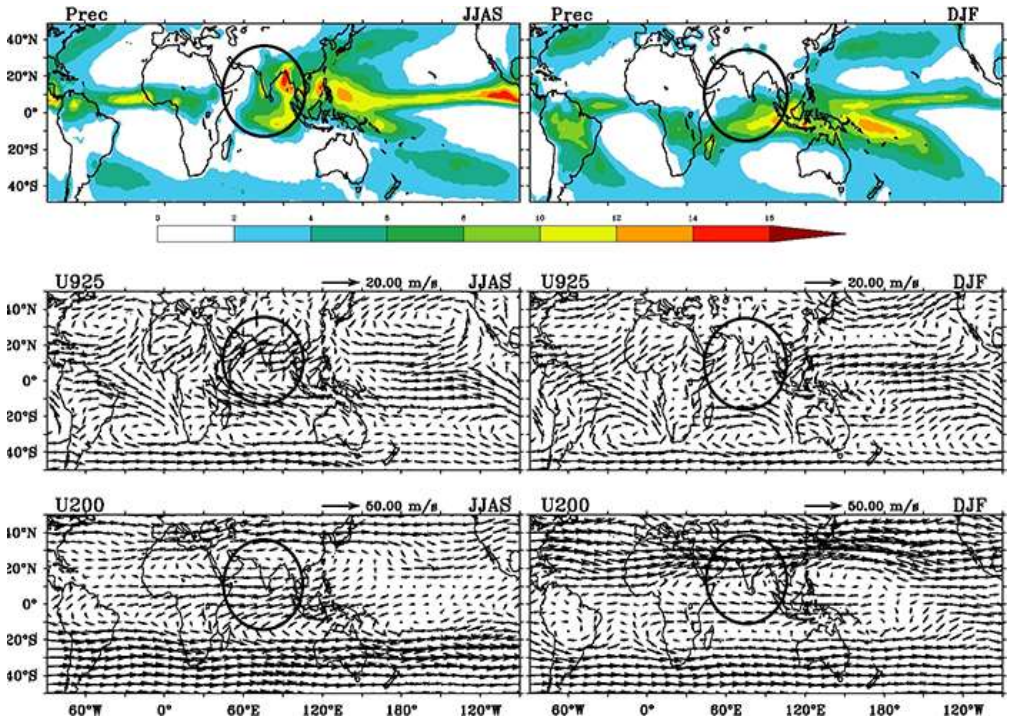

Figure 7: Climatological mean of CMAP precipitation (mm/day, top), NCEP/NCAR reconstructed low-level winds (925hPa, middle), and upper-level winds (200hPa, top) for summer (JJAS) and winter (DJF). Taken from Goswami and Chakravorty, 2017.

Moist static energy (MSE) represents a measure of air parcel instability, making it another useful proxy of convection and indicator monsoon intensity. Analogous to equivalent potential temperature, MSE is a conserved thermodynamic variable that measures an air parcel's enthalpy due to its internal energy due to temperature, its potential energy due to its height above ground, and its latent energy due to water vapor present in the parcel. MSE (typically given in J/kg or kJ/kg) is given by the following formula:

Figure 8: "Arabian Sea" region as defined by Shankle:5-25N, 55-75E for the purpose of area-averaging certain moisture-related monsoon indices.

$$MSE = C_P \cdot T + g \cdot z + L_v \cdot q \quad [4]$$

where C_P is specific heat at constant pressure, T is the absolute air temperature, g is the gravitational constant, z is the height above surface, L_v is the latent heat of vaporization, and q is specific humidity ("Moist Static Energy", American Meteorology Society Glossary of Meteorology). Given that the NCL language used in this study is not currently equipped to calculate convective available potential energy (CAPE), MSE offers a useful alternative indicator of stability and buoyancy. A seminal study by Neelin and Held (1987) showed the usefulness of a vertically-integrated quantity of MSE, which they called "gross moist stability", in simple models of tropical convergence and precipitation patterns. We, however, find a different and arguably more intuitive MSE index to effectively reconstruct parcel buoyancy and instability associated with the Indian monsoon. When the MSE profile of an atmospheric column is characterized by a non-monotonic increase in MSE (exhibiting a decrease in MSE with height before increasing steadily), the column will be unstable and subject to convection; this is because a parcel of air from a lower level, when brought up to a higher level, would be more energetic than the air surrounding it (Figure 9). We define an MSE index as the difference between the area-averaged MSE quantity at 925hPa minus that at 700hPa in order to capture this dynamic. With this index, unstable conditions (prone to convection) during the monsoon season should give large, positive values of the index (MSE at 925hPa > MSE at 700hPa), while more stable conditions during other times of the year would give smaller or even negative values of this index (MSE at 925hPa < MSE at 700hPa). We take this MSE index over both the "All

India" and "Arabian Sea" regions defined previously (Figure 5, Figure 8), for the purposes of this study, as we expect the greatest convection to be occurring over India's landmass and understand the bulk of the monsoon's moisture to arrive off of convection and evaporation over the Arabian Sea to the west.

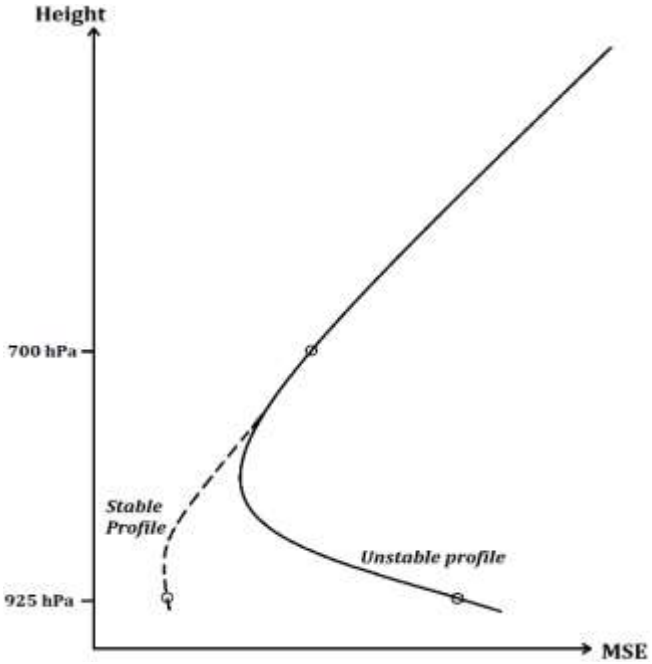

Figure 9: - Diagram of moist static energy profiles for stable and unstable conditions.

4.2.7. Indian Land Surface Temperature, Arabian Sea Surface Temperature, and the Land-Sea Temperature Gradient

The reversal of winds in the summer months that characterizes the Indian monsoon season is believed to be driven by, to a first order, the strong land-sea surface temperature gradient that develops in India in the summer months. In May through June, the accelerated warming of the Indian landmass relative to the cool ocean temperatures to the south produces a low-pressure center over India, forcing a strong southwesterly flow as winds converge toward this low (Goswami and Chakravorty, 2017). We therefore have developed indices tracking India land surface temperatures, ocean temperatures (over the Arabian Sea, from which much of the monsoon's moisture flux originates and which would be consistent with some other indices of this study), and, from these two indices, the land-sea temperature gradient (LSTG). Following the example of past literature on the temperature changes in India and the Indian Ocean, we modeled our India land temperature index on that of Basha et al. (2017) and took the area-average (over the "All India" region, Figure 5) of 2m height temperature anomaly to the mean value of a 1982-2016 base period. Our SST index of the India Ocean is area-averaged over the Arabian Sea with the "Arabian Sea" index mentioned previously, as this is the primary source of monsoon moisture and is similar to other studies on Indian Ocean-sector warming (Roxy et al., 2014).

4.3. ENSO Indices

4.3.1. Niño-SST Region 3.4

The most common ENSO indices used today are sea surface temperature (SST)-based indices that measure anomalies to climatology averaged over some defined region of the Pacific. Four Niño regions have been defined and classified by the National Center for Atmospheric Research (NCAR), the University Corporation for Atmospheric Research (UCAR), and the National Oceanic and Atmospheric Administration (NOAA), largely based on the work of Dr. Kevin Trenberth (Trenberth, 1997; Trenberth & Stepaniak, 2000). The Niño 1, 2, 3, and 4 regions (Figure 10) correspond to labels assigned to ship tracks crossing these regions historically; this allows for historic records of El Niño to be constructed back to 1949 (Rasmusson & Carpenter, 1982).

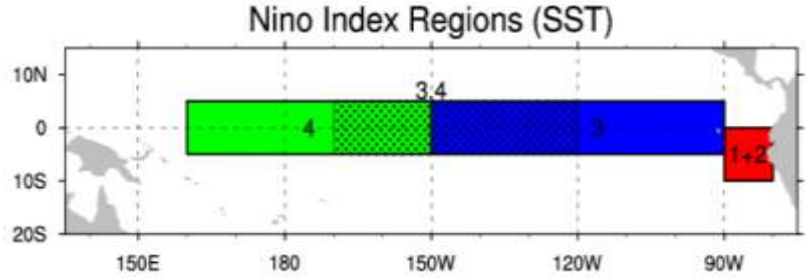

Figure 10: Most commonly used regions to study track ENSO by way of area-averaged SST anomalies. Taken from "Niño SST Indices", NCAR UCAR Climate Data Guide.

The Niño 1 and 2 regions (now combined to a single "1+2" region) make up the smallest and eastern-most regions of study of Niño SST variations. These regions are found on the west coast of South America (0-10S, 90W-80W), where local populations first recognized El Niño events, and have the largest variance of all Niño SST indices. The Niño 3 region (5N-5S, 150W-90W) was historically the accepted region for monitoring and predicting ENSO events, but later research showed the most predictive region for coupled ocean-atmosphere interactions lying further to the west (Trenberth, 1997). The Niño 4 region (5S-5N, 160E-150W) was subsequently developed and shows the least variance of all the SST indices, however it is the latest Niño "3.4" region (5N-5S, 170W-120W) that is most widely accepted today. The Niño 3.4 region is understood to better represent the average equatorial SST anomalies across the Pacific, incorporating parts of both the Niño 3 and 4 regions ("Niño SST Indices", NCAR UCAR Climate Data Guide). For the sake of comparison in this study, we have investigated both the Niño 3 and Niño 3.4 regions as indices of ENSO intensity. Trenberth (1997) encourages the use of the 1950-1979 period as the climatology against which to calculate SST anomalies, as the period from 1979 to 1997 appeared to be dominated by warm events. However, since the reanalysis data used in this study only covers from 1982-2016, that period is used as climatology, both out of necessity and for the purpose of internal consistency. Positive values of the index indicate an El Niño event, while negative values indicate a La Niña event.

4.3.2. Oceanic Niño Index (ONI)

A third, more sophisticated Niño SST index is also included in this study. The Oceanic Niño Index (ONI) is NOAA's primary indicator for monitoring ENSO events. The ONI index calculates a 3-month running mean of SST anomalies in the Niño 3.4 region based on a climatology of a centered 30-year period updated every 5 years; an event of +/- 0.5oC is used to signal an El Niño or La Niña event, respectively (Dahlman, 2009). Again. since the reanalysis dataset used in this study is limited to 1982-2016, we take that period as a constant climatology against which we calculate SST anomalies and the ONI index. Again, positive values of the index indicate an El Niño event, while negative values indicate a La Niña event.

4.3.3. Southern Oscillation Index (SOI) and Equatorial Southern Oscillation Index (ESOI)

Before SST-based indices became popular and practical to measure in studies of ENSO, the historical precedent was the use of indices based on sea level pressure (SLP). In fact, the oldest indicator of ENSO is the Southern Oscillation Index (SOI), defined by Walker (1923) and Walker and Bliss (1932) who first observed the "seesaw" in SLP differences between the western and eastern Pacific Ocean. SOI is defined as the difference between the atmospheric pressure at sea level between weather station in Tahiti and Darwin, Australia (Tahiti minus Darwin) (Troup 1965; Torrence & Webster, 1999). A negative SOI value indicates above-average pressure conditions in Darwin and below-average pressure conditions in Tahiti, consistent with an El Niño event. Opposite conditions, and a positive SOI value, accompany La Niña events. This SLP difference can be standardized to a long-term mean difference between the two stations, however Troup (1965) established that a simple difference in SLPs at the two stations was a robust enough indicator of the oscillation. Given that the reanalysis data used in this study is gridded, the SOI index presented here is given as the SLP values at the grid points closest to the latitude and longitude locations of the Tahiti (17.6S, 210.4E) and Darwin (12.4S, 130.9E) weather stations (Figure 11, left).

For purposes of thoroughness and for its greater compatibly with a gridded dataset over single-point weather stations, the Equatorial Southern Oscillation Index (ESOI) was also developed to measure ENSO intensity. NOAA refined the original SOI index by using the standardized difference in average sea level pressure over two large regions centered on the equator (5S-5N) over Indonesia (90-140E) and the eastern Pacific (230-280E) (Pacific minus Indonesia) (Barnston, 2015, NOAA Climate.gov; "Southern Oscillation Index (SOI) and Equatorial SOI",

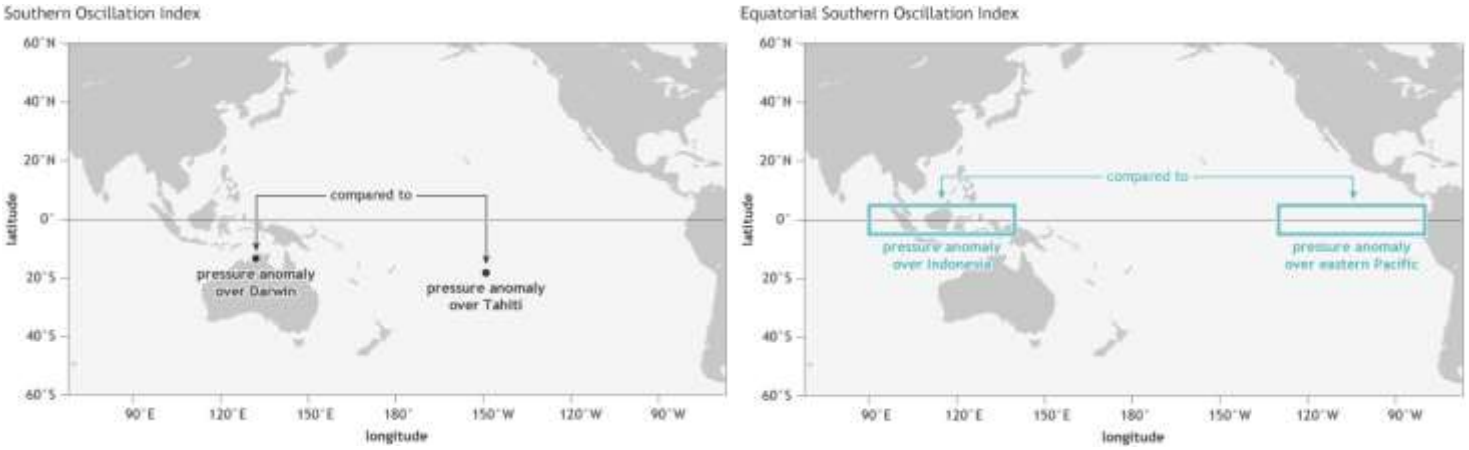

Figure 11: SOI weather stations and ESOI regions. Taken from Barnston, 2015, NOAA Climate.gov.

International Research Institute for Climate and Society, Columbia University). The ESOI index makes two significant improvements to the historical SOI index. First, the SOI index, being based on the SLP measurements of individual weather stations, can be affected by shorter term (day-to-week) fluctuations unrelated to ENSO. Secondly, the SOI index is somewhat biased for its stations being located slightly south of the equator (Tahiti at ~18S and Darwin at ~12S); the ESOI index is superior for using average SLP over two large regions centered on the equator, where the majority of the ENSO signal manifests. Despite these advantages of the ESOI index, we include the SOI index in our study as well out of conventionality and for the advantage of its longer historical record (to the late 1800s).

4.3.4. Equatorial Outgoing Longwave Radiation

A third category of ENSO indices involve measurements of outgoing longwave radiation (OLR) at the top of Earth's atmosphere across the equatorial pacific. NOAA's Climate Prediction Center the equatorial outgoing longwave radiation index as the area-average of OLR over the entire equatorial Pacific (5S-5N, 160-200E) ("Outgoing Longwave Radiation (OLR), NOAA Climate Prediction Center). Raw data is typically converted into a standardize anomaly to a base period of 1979 to 1995 but given that the reanalysis dataset used in this study starts at 1982, the OLR is reported as absolute values rather than anomalies here. OLR serves as an indicator of ENSO activity since low OLR values are indicative of enhanced convection and cloud coverage typical of an El Niño event. Greater convective activity as a result of elevated, El Niño SSTs in the central and eastern equatorial Pacific in turn implies higher, colder cloud tops which emit less infrared ("long-wave") radiation to space (hence lower OLR values). The opposite is true of a La Niña event – colder SSTs in the central and eastern equatorial Pacific suppress convection,

resulting in lower and warmer cloud tops that emit relatively more infrared radiation ("Outgoing Longwave Radiation (OLR), NOAA National Centers for Environmental Information).

4.4. Warming Indices

4.4.1. Global Mean Surface Air and Sea Surface Temperature Anomalies

Global warming is most intuitively defined in terms of surface-level temperature changes. The indices adopted by NASA and NOAA are largely based on the work of Hansen et al. (2010). Global mean surface air temperature (annual, seasonal, or monthly) is recorded from meteorological station data and interpolated between stations with reanalysis data; the same is done for sea surface temperature (SST) data from buoys, floats, and (since the 1970s) satellite measurements ("GISS Surface Temperature Analysis", NASA. "Extended Reconstructed Sea Surface Temperature (ERSST)", NOAA.). Following the example of Hansen et al. (2010), we reconstruct global mean surface air temperature anomalies by averaging reanalysis surface air temperature globally and taking the anomaly to the mean value of the 1951-1980 base period (not include in our reanalysis dataset but reported as 14^{o}C by Hansen et al. 2010). Similarly, we reconstruct global mean SST anomalies by averaging SST values across total ocean surface area and calculating anomalies against the mean value of the 1981-2016 base period (the entirety of our reanalysis dataset, in contrast to the 1971-2000 base period used by NOAA).

4.5. IOD Index

4.5.1. Dipole Mode Index (DMI)

The most common index to measure the Indian Ocean Dipole is the Dipole Mode Index (or DMI), which is defined as the difference in SST anomaly between the western (10S-10N, 50-70E) and southeastern (10S-equator, 90-110E) equatorial Indian Ocean (Saji et al., 1999). Saji, the author of the seminal paper on the Indian Ocean Dipole (1999), does not specify the base period from which to calculate a climatology for the calculation of anomalies, but the Indian National Centre for Ocean Information Services takes 1981-2010 as its period, while NOAA's Ocean Observations Panel for Climate takes the period as 1982-2005. We take the base period of 1982-2010 for its longer time span ("Status of IOD"; "Dipole Mode Index (DMI)").

4.6. Summarizing Table of Indices

The following table summarizes the definitions and significance of each of the indices used in this study. Where indices are previously well-established in literature or in practice, the relevant

TABLE 1 – INDICES FOR THE INDIAN MONSOON, ENSO, GLOBAL WARMING, AND IOD				
"Seasonal Signal"			**Units**	**Significance**
Solar Irradiance	**solar_rad**	Area-averaged downward longwave radiation at top of atmosphere over "All India" region (Shankle, 10-35N, 65-95E).	W/m^2	Strong driver of the monsoon, possibly overpowering any effects of other phenomena (ENSO, etc.).
Monsoon				
Extended Indian Monsoon Rainfall	**EIMR**	Area-averaged precipitation over 70-110E, 10-30N. (Goswami et al., 1999).	mm/mo	Most obvious and relevant index of monsoon intensity.
Zonal Vertical Shear	**vert_shear_u**	Area-averaged zonal velocity over "All India" region (Shankle, 10-35N, 65-95E), difsference between 200hPa level minus 850hPa level.	m/s	Measure of the magnitude of reversal of winds, a fundamental characteristic of monsoon season.
Velocity Potential (200hPa)	**vp200**	Area-averaged velocity potential over "All India" region (Shankle, 10-35N, 65-95E) at the 200hPa level.	m^2/s	A measure of air flow convergence/divergence, a proxy for sinking or rising air (convection).
Velocity Potential (850hPa)	**vp850**	" " the 850hPa level.	m^2/s	
Mid-Tropospheric Relative Humidity (avg. 400-700hPa)	**rhavg400700**	Area-averaged relative humidity over "All India" region (Shankle, 10-35N, 65-95E), averaged over 400-700hPa.	%	A proxy for moisture flux into the atmospheric column and propagation of monsoon front over India.
Moisture Flux, India	**MF_Ind**	" " over the "All India" region (Shankle, 10-35N, 65-95E).	kg/(ms)	Measure of enhanced moisture transport into the India sector, providing moisture to drive the monsoon.
Moisture Flux, Arabian Sea	**MF_Arab**	Area-averaged total-column zonal moisture flux over the "Arabian Sea" region (Shankle, 5-25N, 55-75E).	kg/(ms)	
Moist Static Energy Index (925hPa – 700hPa), India	**MSE_Ind**	Area-averaged moist static energy over "All India" region (Shankle, 10-35N, 65-95E), difference between 925hPa level minus 700hPa level.	J/kg	Measure of atmospheric stability, a proxy for rising air (convection).
Moist Static Energy Index (925hPa – 700hPa), Arabian Sea	**MSE_Arab**	" " area-averaged over the "Arabian Sea" region (Shankle, 5-25N, 55S-75N).	J/kg	
Indian Land Surface Temperature	**Ind_temp**	2m air temperature averaged over the "All India" region (Shankle, 10-35N, 65-95E).	degC	Component of the land-sea temperature gradient understood to be a primary driver of the monsoon.
Arabian Sea Surface Temperature (SST)	**Arab_temp**	Area-averaged SSTs over the "Arabian Sea" region (Shankle, 5-25N, 55S-75N).	degC	
Land-Sea Temperature Gradient	**LSTG**	Difference between the Ind_temp minus Arab_SST indices.	degC	Conventionally understood to be the primary driver (at least to a first-order) of the Indian monsoon.
ENSO				
Niño-SST Region 3.4	**nino_34**	Area-averaged SST anomaly to the dataset's climatology (12/1981-08/2017), over the Niño-3.4 region (5S-5N, 190-240E). (Trenberth, 1997).	degC	Main signal of an ENSO event.
Oceanic Niño Index (ONI)	**ONI**	Area-averaged (Niño-3.4 region), 3-month running average of SST anomaly to the dataset's climatology (12/1981-08/2017); +/- 0.5ºC signals an event. (NOAA.)	degC	Same as Niño 3.4 index but standardized with a 3-month running mean, the index preferred by NOAA.
Southern Oscillation Index (SOI)	**SOI**	Sea-level pressure difference between weather stations in Tahiti (17.6S, 210.4E) minus Darwin (12.4S, 130.9E). (Torrence and Webster, 1999; Troup, 1965). Approximated with the grid cell closest to each station.	Pa	The historical ENSO index originally developed by Walker (1923), who first observed the oscillation of atmospheric pressure between Tahiti and Darwin.
Equatorial Southern Oscillation Index (ESOI)	**ESOI**	Area-averaged standardized sea-level pressure anomaly to the dataset's climatology (12/1981-08/2017), difference between Eastern Pacific (5S-5N, 230-280E) minus Indonesia (5S-5N, 90-140E). (NOAA.)	Pa	A refinement of the SOI index, standardized and area-averaged over the equator, preferred by NOAA.
Equatorial Outgoing Longwave Radiation	**eq_OLR**	Area-averaged outgoing longwave radiation anomaly to the dataset's climatology (12/1981-08/2017) over 5S-5N, 160-200E. (NOAA.)	W/m^2	A measure of convection and cloud production, a new ENSO index with the advent of satellite-based data.
Global Ocean Warming				
Global Mean Surface Air Temperature Anomalies	**glob_temp_anom**	Globally-averaged 2m air temperature, anomalies to the dataset's climatology (12/1981-08/2017). (NASA.)	degC	A measure of warming over the entire surface of the Earth.
Global Mean Ocean SST Anomalies	**glob_SST_anom**	Globally-averaged SST anomalies to the dataset's climatology (12/1981-08/2017). (Hansen et al., 2010; NASA.)	degC	A measure of ocean warming across the Earth.
IOD				
Dipole Mode Index	**DMI**	Area-averaged SST anomaly to climatology (12/1981-08/2017), difference between W equatorial Indian Ocean (10S-10N, 50-70E) minus SE equatorial Indian Ocean (10S-0N, 90-110E). (Saji et al., 1999).	degC	A measure of the west-east SST gradient within the Indian Ocean, the conventional index of the IOD.

citation is included. A map showing the areal extent of most of the area-averaged indices is shown in Figure 12.

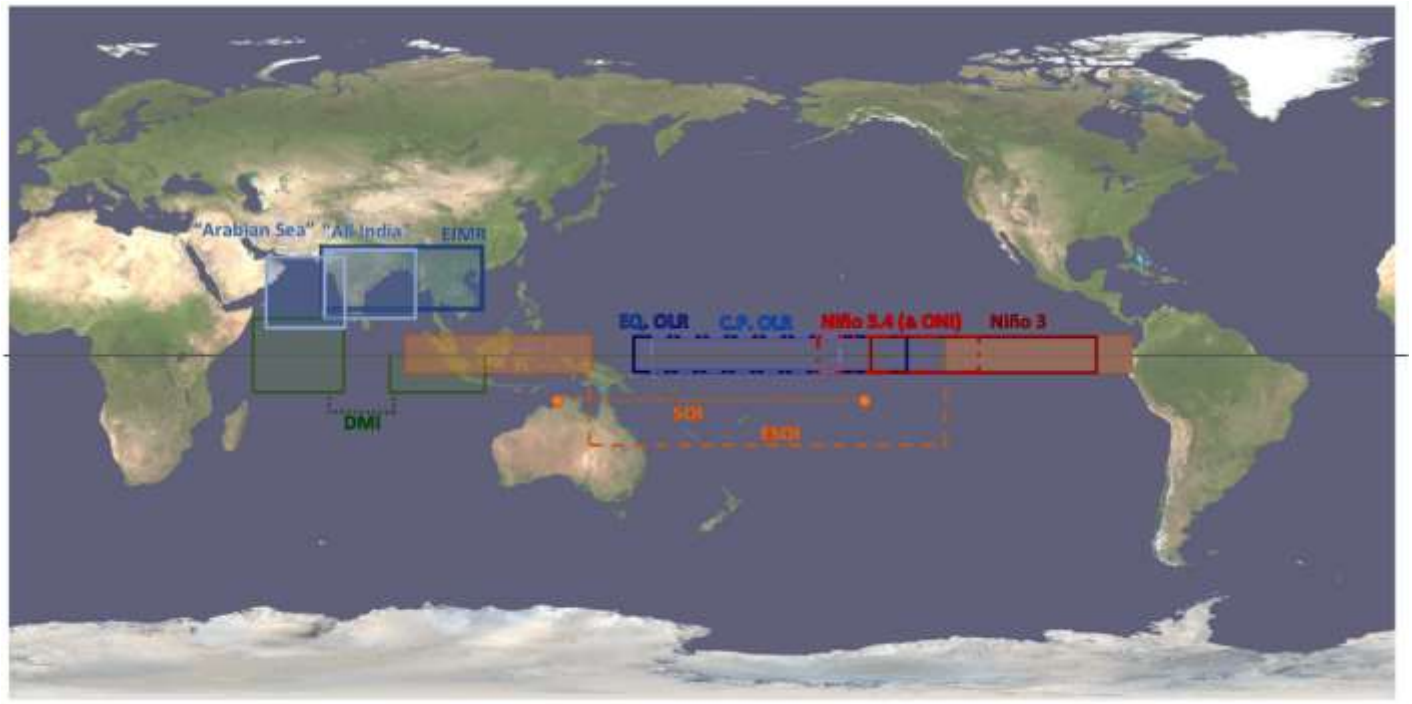

Figure 12 - Area extents of the area-averaged indices of this study.

5. Times Series of the Indices

The indices were first plotted in monthly time series to assess their ability to capture basic patterns of the four climate phenomena assessed in this study. The monthly time series of a few demonstrative indices of each climate phenomena are given in Figure 13. In this figure, monthly values of the indices are given in red curves while the climatological monthly variation of each index is given in black. The time period of 2006 to 2016 was chosen for this figure both for brevity and to capture important historical events such as the strong 2015 El Niño and the strong 2010 La Niña. For ENSO and IOD indices, red and blue shading indicates weakening and strengthening influences on the monsoon, respectively. For the ENSO indices, these colors also represent El Niño (red) versus La Niña (blue) events.

In these time series, all indices appear to be quite robust at capturing well-constrained patterns associated with the various phenomena. The best example of this is the obvious seasonal cyclicity of the monsoon indices (for example, Fig.13 a-d). Climate variables that are observed to intensify every summer with the onset of the monsoon do so in each of the indices, before declining again in winter months. Similarly, the indices accurately recreate observed

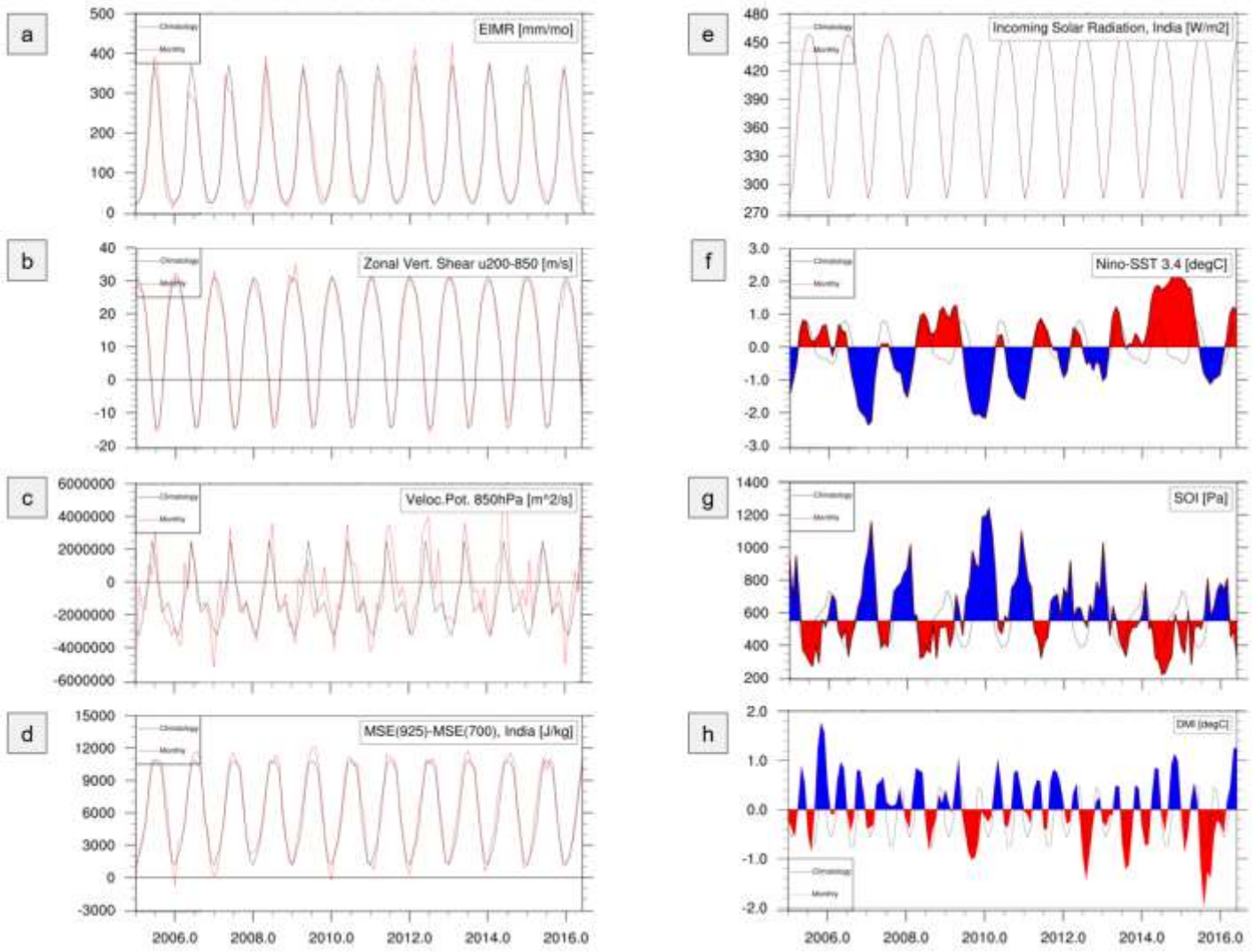

Figure 13: Monthly time series of representative indices from each of the climate phenomena. The interval of 2006-2016 was chosen as representative and for the purpose of brevity. This interval also contains important demonstrative historical events such as the 2015 El Niño and the 2010 La Niña.

interannual variations of ENSO and the IOD (for example, Fig. 13 f-g) and capture such important historical events as the strong El Niño and La Niña events of 2015 and 2010, respectively. There is even the semblance of an inverse relationship between the Nino-SST 3.4 and DMI indices – with positive (blue) IOD events accompanying intervals of El Niño (red) events and negative (red) IOD events accompanying years of La Niña (blue) events – that has been postulated by recent studies (Forootan et al., 2016). Global warming indices (not pictured in Fig. 13) are also consistent with well-established records of global warming, showing an increasing trend in recent decades (Hansen et al., 2010; NOAA; NASA).

Special attention is drawn to the time series of incoming solar radiation (Fig. 13 e). The cycle of incoming solar radiation is an artefact of the eccentricity, obliquity, and precession of the Earth's orbit and is the mechanism responsible for Earth's seasons. Given the long time scales (tens to

hundreds of thousands of years) at which these orbital processes vary, the pattern of incoming solar radiation over any given location on Earth is essentially consistent from year to year on the short time scales of this study. This is demonstrated by the perfect overlap of the monthly time series (red) and the climatology (black) of this index in Fig. 13 e. It is this consistent variation in incoming solar radiation throughout the year that drives the Earth's seasonal cycle and thus poses a problem in the statistical analysis of this study; to one extent of another, all the indices considered here will have some degree of seasonality. The seasonal cycle of the monsoon indices is obvious, but the indices of ENSO and the IOD – being based either directly or indirectly on sea surface temperature and sea level pressure anomalies – will also experience the influence of the seasonal cycle. Thus, the signal of the seasonal cycle represents a confounding variable in this study. We suspect that it would artificially increase correlation coefficients between monthly values of any two indices, which may possibly be unrelated but appear correlated by nature of seasonal fluctuations they both experience. To account for the effect of the seasonal cycle, in subsequent analysis we consider both monthly values of the indices, as well as the time series of annual June-July-August (JJA)-averages across the dataset (Figure 14). By consistently taking only the summer values of these indices, we effectively eliminate the influence of the seasonal cycle, thus enabling us to better assess inherent correlations between the climate phenomena.

This concept is demonstrated and the time series of the JJA values of the indices given in Figure 14. This figure shows the times series of same demonstrative climate indices as Figure 13 – but in their annual JJA values rather than monthly values – across the entire dataset (1982 to 2016). The virtually-constant value of incoming JJA solar radiation (Fig. 14 e) demonstrates how the seasonal cycle is not a factor in these time series. This data, then, allows us to track interannual variations in the indices, as well as correlate them more robustly without the confounding influence of the seasonal cycle. Aside from this, we observe the indices again capturing certain fundamental features of each of the four climate phenomena. We observe strong evidence of ENSO's 5 to 7-year frequency in the indices (Fig. 14 f, g) as well as the higher-frequency variation (roughly interannual) of the IOD (Fig. 14 h). In the monsoon variables (Fig. 14 a-d), we see perhaps some evidence of an interannual cyclical cycle in monsoon intensity, although this is not a dynamic that has been readily demonstrated in the monsoon in any past literature. We observe no significant trends over the dataset, except in the global warming indices (not pictured in Figure 14), which as in the monthly time series show increasing surface temperatures. The objective of this study, however, is not to establish temporal trends in these indices; rather it is to

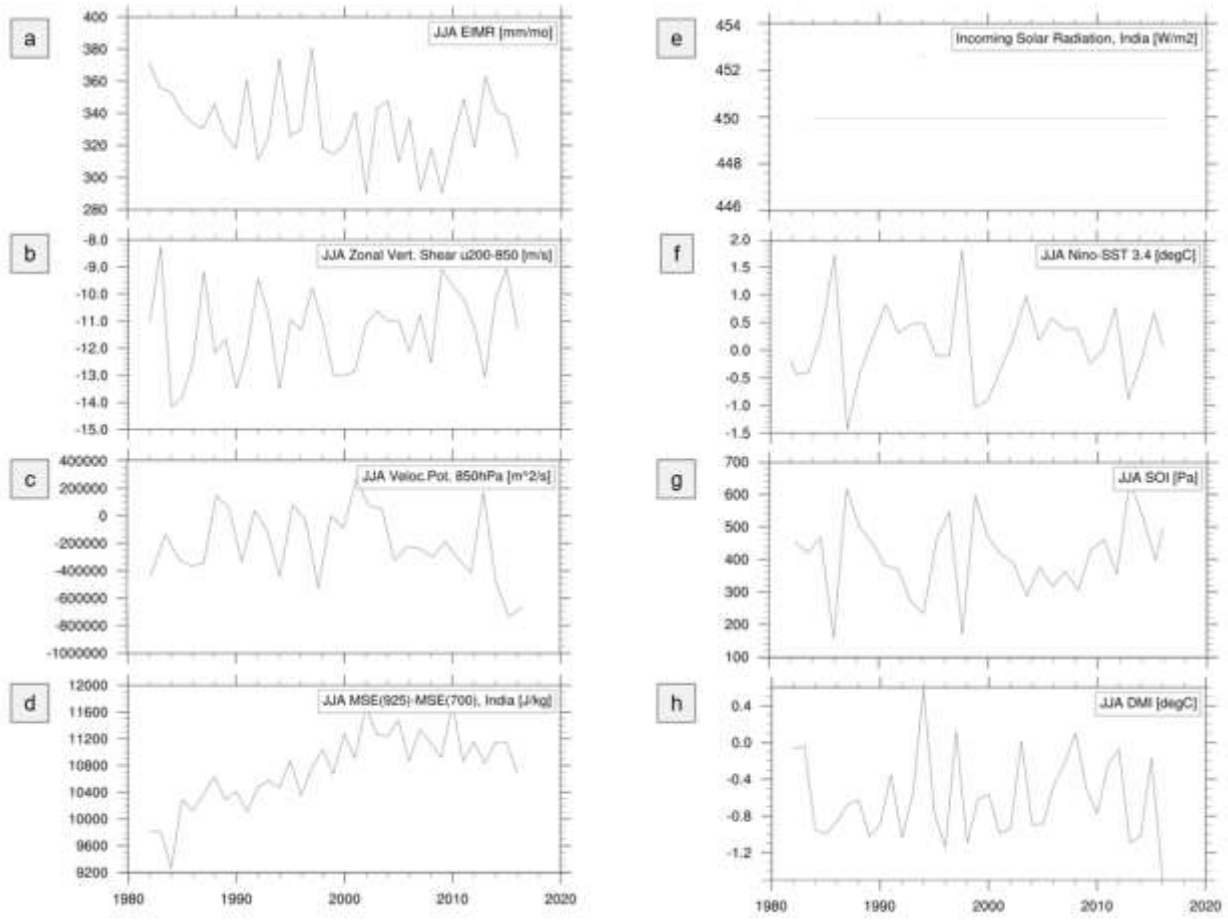

Figure 14 – Annual values of June-July-August (JJA)-averaged values of the same representative indices of the climate phenomena as used in Figure 13, across the entirety of the data set (1982-2016).

assess the statistical correlation of these indices in an attempt to illuminate relationships between the monsoon and other climate phenomena. Having removed the effect of the seasonal cycle by taking the JJA values of the indices, we are now prepared to pursue this statistical analysis. The time series plots in this section have served both to illustrate that removal of the seasonal signal in the JJA values, as well as to demonstrate the robustness of the indices in capturing basic climate patterns associated with these phenomena.

6. Statistical Analysis

Various statistical analyses were performed on the data before calculating correlation coefficients between the indices. First, the normality of the indices' distributions was assessed through an inspection of their skewness and kurtosis (degree of "flatness") values; distributions deviating from a Gaussian distribution can indicate certain patterns or tendencies in the respective climate phenomena. Next, the bimodality of the indices distributions was calculated through two coefficients – the Sarle's bimodality coefficient and the finite sample bimodality

coefficients. This analysis will capture any bimodal frequencies to the indices – whether from the seasonal cycle or otherwise. Further details on the procedure of calculating skewness, kurtosis, and bimodality in the indices is given in the appendix (A2. Statistical Methods). These two analyses – the assessment of normality and bimodality – complement the final analysis performed on the data, which was a calculation of correlation coefficients between all indices. The following section is split into the monthly (seasonal) cycle of the indices and the interannual JJA values of the indices. Observations of various statistical features of these two versions of the data will be discussed in great detail here but summarized and discussed in terms of their significance in the Conclusions section. The statistical trends in the monthly time series of the data will be discussed first.

6.1. Monthly Values (The Seasonal Cycle)

6.1.1. Normality of the Indices' Distributions

Figure 15 plots the skewness and kurtosis values of the distribution of monthly values in each index. Means, standard deviations, and values of skewness, kurtosis, and bimodality are summarized in Table A1in the appendix (A2. Statistical Tables – Skewness, Kurtosis, and Bimodality, and Correlation Coefficients). Positive and negative values of skewness indicate strong rightward and leftward tails to the distributions, respectively, with a value of 0 indicating perfect symmetry (a characteristic of the normal Gaussian distribution). Positive values of kurtosis indicate distributions that are more sharply peaked than a Gaussian distribution, while negative values indicate a distribution flatter than a Gaussian distribution.

The indices' distributions span a wide, disperse cloud of skewness and kurtosis values, indicating a tendency towards distributions that deviate from the normal distribution. The first main observation is a trend towards negative (flatter-distribution) kurtosis values. This is interpreted to be an artefact of the seasonality of many of these indices. Having distinctly diverging average values between summer and winter months, most of these indices cover a wide range of values, resulting in a distribution wide and flatter than that of the normal distribution. The second observation of this figure is a trend toward positive (right-tailed) skewness in all the indices except those of ENSO. The positive skewness values of the monsoon indices are interpreted to be the result of the extreme monsoon months (June, July, and August) "pulling up" the distributions from their mean, less extreme values in the rest of the months in the year. The occasional opposite skewness of monsoon indices (namely vertical shear, India land temperature,

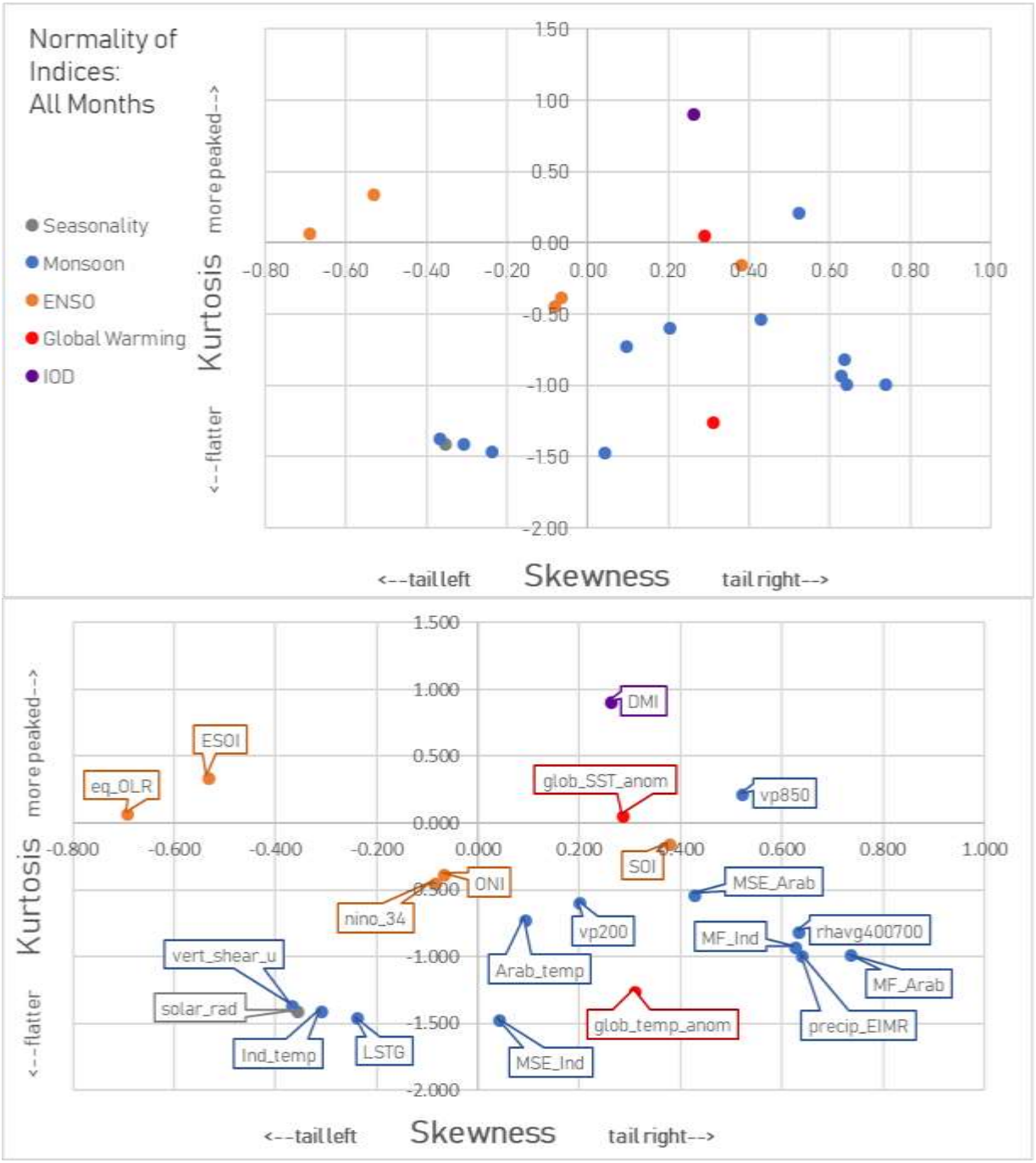

Figure 15: Plot showing the skewness and kurtosis values of the distributions of the indices' monthly values across the data set.

or the land-sea temperature gradient) is either the result of the definition of these indices (in the case of the vertical shear, which is reversed with every monsoon season) or of bimodality in these indices' distributions (explained in the next section). The global warming and DMI indices show positive skewness values, as well, and this is tentatively interpreted as a result of the increasing trend in temperatures making positive anomalies from the mean (and thus rightward skew in the distributions) more likely than negative anomalies in surface temperature (and in ocean temperature, which might be influencing the DMI index). The ENSO indices are the only

ones to exhibit both positive and negative skewness with no clear reason; in fact the SOI and ESOI indices, which are two iterations of the same measurement, show opposite-signed skewness (0.375 and -0.536, respectively). The interpretation of this can only be speculated at, but perhaps the SOI and ESOI indices, being located in slightly different geographic locations, experience the influences of different, unexplained phenomenon not addressed in the literature thus far.

In either case, we hypothesized that skewness and kurtosis would both be reduced in the indices JJA distributions of JJA in which the effect of the seasonal cycle was removed. Skewness was found to be reduced, while kurtosis was not (discussed in section 6.2.1).

6.1.2. Bimodality of the Indices

The vast majority of monsoon indices exhibit bimodality in their distributions, surpassing the thresholds of the Sarle's and finite sample bimodality coefficient thresholds of 0.5 and 0.555 (Table A1). This is interpreted to be a result of the strong seasonality of these indices. We expect these indices to be clustered around two populations of values – monsoon season values and non-monsoon season values (the rest of the year). These two peaks are very visible in the distributions of the indices displayed in Figure 16, which shows the indices with the highest bimodality values. Velocity potential at 850hPa and equatorial outgoing longwave radiation are the only two indices to qualify as bimodal by the calculated coefficients but not appear bimodal in their distributions, leading us to assume that these coefficients are robust at predicting truly bimodal populations of values in the indices. Again, we expect the bimodality of the indices to decrease with the removal of the seasonal cycle, and it slightly was (discussed in section 6.2.2).

6.1.3. Correlations between Indices

The final statistical analysis performed on the data was the calculation of correlation coefficients. The most obvious observation to be taken from the table of correlation coefficients (Table A3) is the correlation of indices of a given climate phenomenon being well correlated with themselves (this being particularly true of the monsoon and ENSO variables). This is not unexpected but still significant for demonstrating how robust these indices are for tracking a given climate phenomenon; despite being based on a variety of physical variables, their strong correlations demonstrate their relatedness to each other and robustness in all tracking the same process. The second observation to be made is the strong correlation (>0.6) of incoming solar radiation with the majority of monsoon indices (nine out of twelve) but none of the ENSO, warming, or IOD

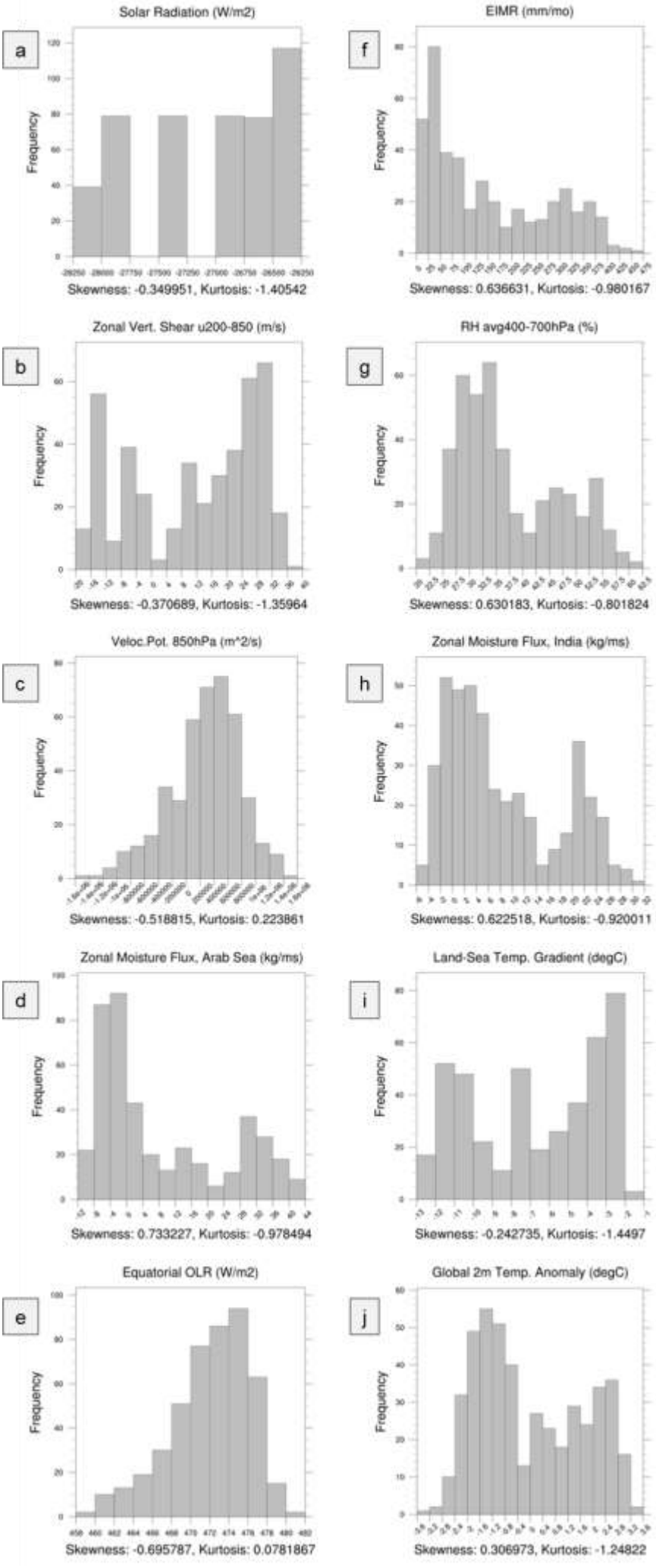

Figure 16: Distributions of the monthly values across the dataset of the indices with the top ten highest bimodality coefficients.

indices (except global warming). This simply demonstrates the strength of the seasonal cycle in influencing the monsoon variables, since incoming solar radiation represents the primary seasonal forcing of the monsoon. As will be shown in the next section, this strong tracking of monsoon indices and solar radiation is greatly reduced amongst JJA values (Table A3), allowing other significant trends to be revealed. Additionally, there is no strong correlation observed between the monsoon and the ENSO or IOD variables. Perhaps at monthly time scales, the strong seasonality of the monsoon indices is incompatible with the interannual nature of ENSO and the IOD.

We also observed a constant pattern of high correlation with the global land surface temperature anomaly with all but one of the monsoon indices; the reason for this could not be determined but could be the result of a failure to take monthly anomalies of the global surface temperatures. Even so, however, the correlation values are exceptionally high (commonly > 0.8 and occasionally being as high as 0.92), and so we suspect that this is some other mistake in the data (the code could not be successfully debugged at the time of submission of this thesis).

6.2. JJA Values (Interannual Variation)

6.2.1. Normality of the Indices' Distributions

Figure 17 (and Table A2) shows the distributions of most indices (in annual JJA values) being usually flatter than a normal distribution, as indicated by the clustering of points in negative kurtosis values. This pattern is persistent across all four climate phenomenon, as well as in the cycle of solar radiation (labeled as "Seasonality" in Figure 17). The skewness is also greatly reduced compared to the indices' distributions of monthly values, indicating greater symmetry in these distributions. The greater symmetry is attributed to having removed the effect of the seasonal cycle; the distributions of monthly values in the indices are now no longer skewed one direction or another by the three intense summer/monsoon months out of the year or by two populations of values clustered about summer and winter means. However, the retention of relatively high negative kurtosis values (>-0.5, comparable to those of the distributions of monthly values mentioned previously) is indicative of the indices still spanning a relatively large range of values, even in this interannual variation. Some of this "flatness", however, can be attributed to some lingering bimodality, as will be discussed in section 6.3.1.

The only exceptions to these observations are the DMI and ESOI indices, which show increased rather than reduced positive and negative skewness (>0.5), respectively, and the land-sea

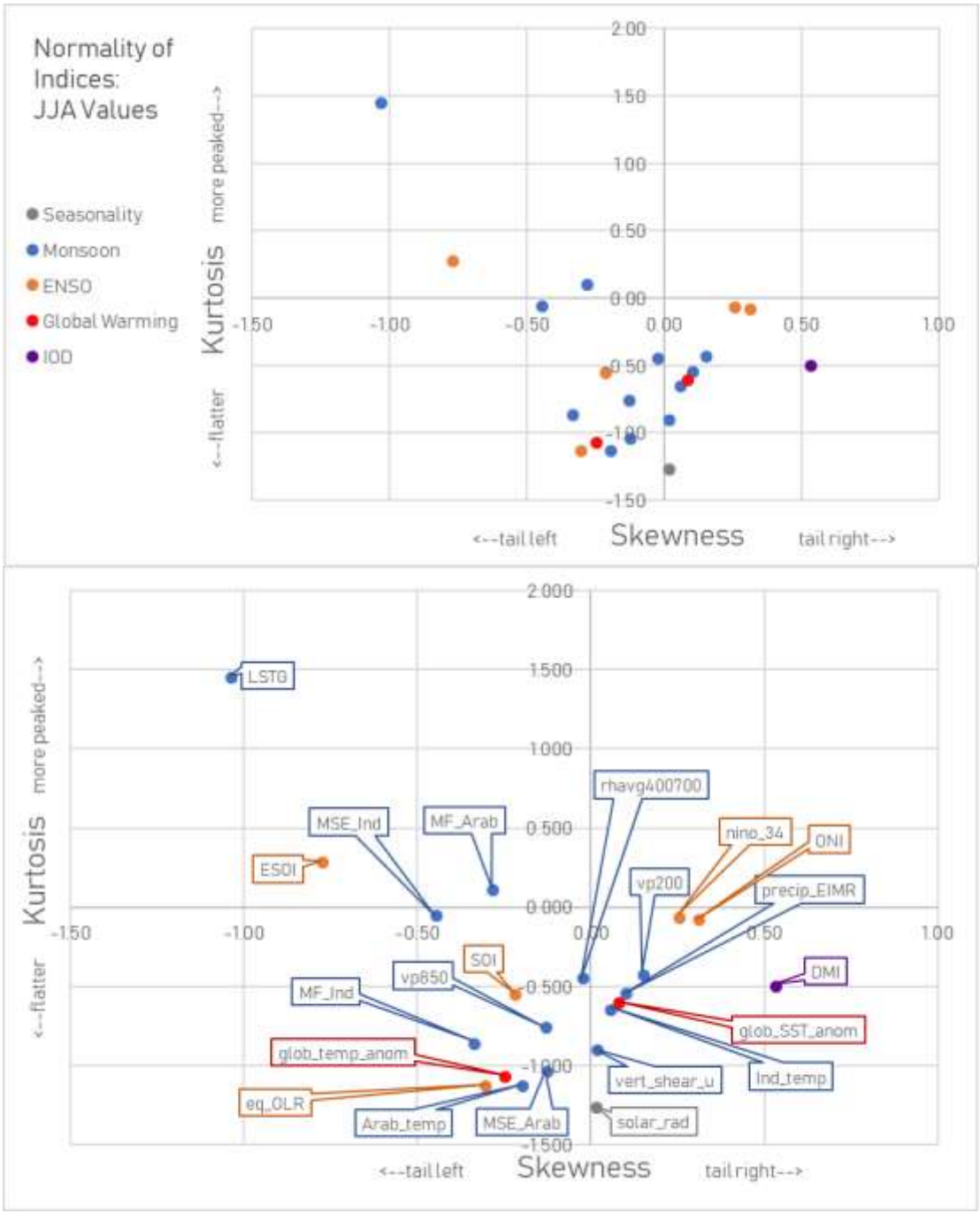

Figure 17: Plot showing the skewness and kurtosis values of the distributions of the indices' monthly values across the data set.

temperature gradient (LSTG), which shows both strong (negative/leftward) skewness and strong (positive/peaked) kurtosis. The positive and negative skewness values of the DMI and ESOI indices indicate tails on their distributions to the right and the left, respectively. This could be the result of these indices being more sensitive than others to occasional extreme values that drag out their distributions in either direction. It is impossible to ascertain from this data, however, as to what sorts of influences would be responsible for this heightened sensitivity in these indices. The

skewness and kurtosis values of the LSTG indicate its distribution being sharply peaked (narrow) with a strong leftward tail. Such a narrow distribution indicates the LSTG's values clustering around a narrow range of values and thus perhaps hints at the LSTG being a phenomenon with relatively small variation. The strong leftward tail indicated by its negative skewness value (-1.44), however, also perhaps indicates the occasional event of a low LSTG dragging the distribution towards those lower values. The lack of a rightward, positive tail might indicate it being difficult for the LSTG to experience strong positive anomalies (perhaps due to some threshold of warming that can be experienced by the land or the ocean), while its strong leftward tail perhaps indicates the prevalence of occasional negative anomalies in the LSTG.

6.2.2. Bimodality of the Indices

As expected, the bimodality of the indices is reduced in virtually all cases by having removed the effect of the seasonal cycle (Figure 18). Only three monsoon indices retain their bimodality, as does incoming solar radiation. However, while bimodality is reduced, it is not completely eliminated from any of the indices. This is an intriguing finding as we expect a variable to be bimodal as a result of one of two factors: either bimodality in its forcing or intrinsic bimodality inherent to its own dynamics. Having removed the bimodal forcing (the seasonal cycle) in these JJA values, the retention of bimodality in some of the indices hints at the existence of a natural, bimodal state in these indices – inherent to the dynamics of the system itself and outside of the influence of the seasonal cycle. Interestingly, a greater proportion of the monsoon variables display bimodality than do the ENSO variables, even though ENSO is manifested in apparently two "end-member" events (namely the El Niño and the La Niña). These results corroborate the view of ENSO being more of a spectrum of states than a bimodal system tending towards two distinct endmembers, and they suggest that perhaps the monsoon conversely tends towards two fundamental states more so than being a spectrum of conditions. The view of ENSO as a spectrum is perhaps more correct than the view of it as two distinct states – the El Niño condition or the La Niña condition – since the definition of such an event is based on an arbitrary threshold hold of an anomaly (such as a +/-0.5^{o}C anomaly in the Niño-3.4 SST index), when in reality the index spans a whole range of states on a yearly basis. This data, however, is relatively unprecedented in suggesting any degree of bimodality being inherent to the monsoon system.

"Active" and "weak"/"break" spells in the monsoon are an area of active research (Goswami et al., 1998; Goswami and Mohan, 1999), but these only explain fluctuations on the intraseasonal

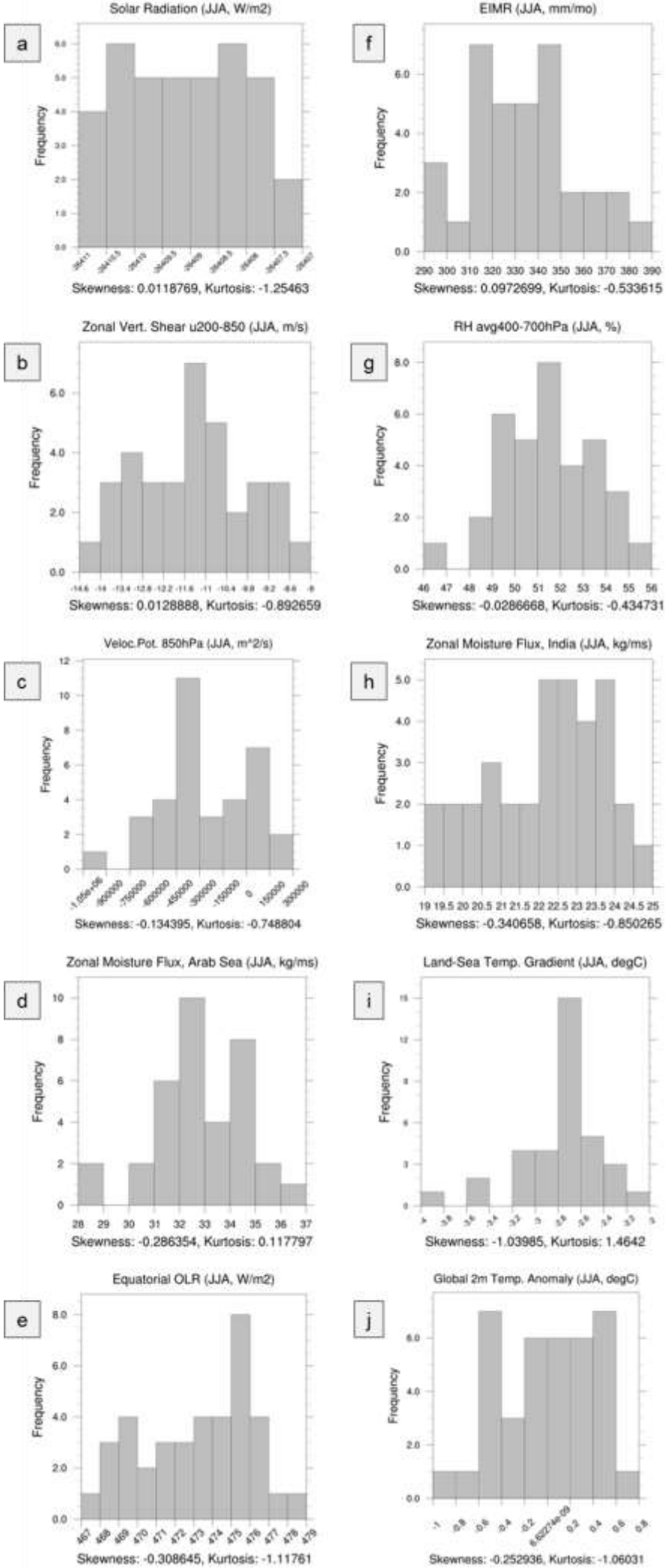

Figure 16: Distributions of the JJA values across the dataset of the indices with the top ten highest bi8odality coefficients.

scale. Outside of this, the closest the present literature comes to attributing quantized states such as this to the monsoon system is the work of Narasimha (Narasimha and Kailas (2001) and Narasimha and Bhattacharyya (2010), who uses wavelet analysis (functions designed to divide a record into differently-scaled components of different frequencies) to study temporal variability of monsoon rainfall. This collection of work has revealed annually-sampled seasonal rainfall data exhibiting statistically significant periodicities of 3, 5.8, 11.6, 20.8, 37, and 80-year periods. Perhaps the bimodality exhibited by the data of this study is related to the same mechanism responsible for these newly postulated oscillations in monsoon rainfall, although rainfall is not one of the indices we observed to qualify as bimodal

A final observation to be made of this data was three indices that surpassed the bimodal threshold only after being reduced to their JJA values (Figure 19). These were the moist static energy difference between 925 and 700hPa over the Arabian Sea, Arabian Sea surface temperatures, and the Dipole Mode Index. The reason for this is not clear, but perhaps these variables vary interannual such that they tend towards two distinct states at interannual timescales but not at monthly timescales.

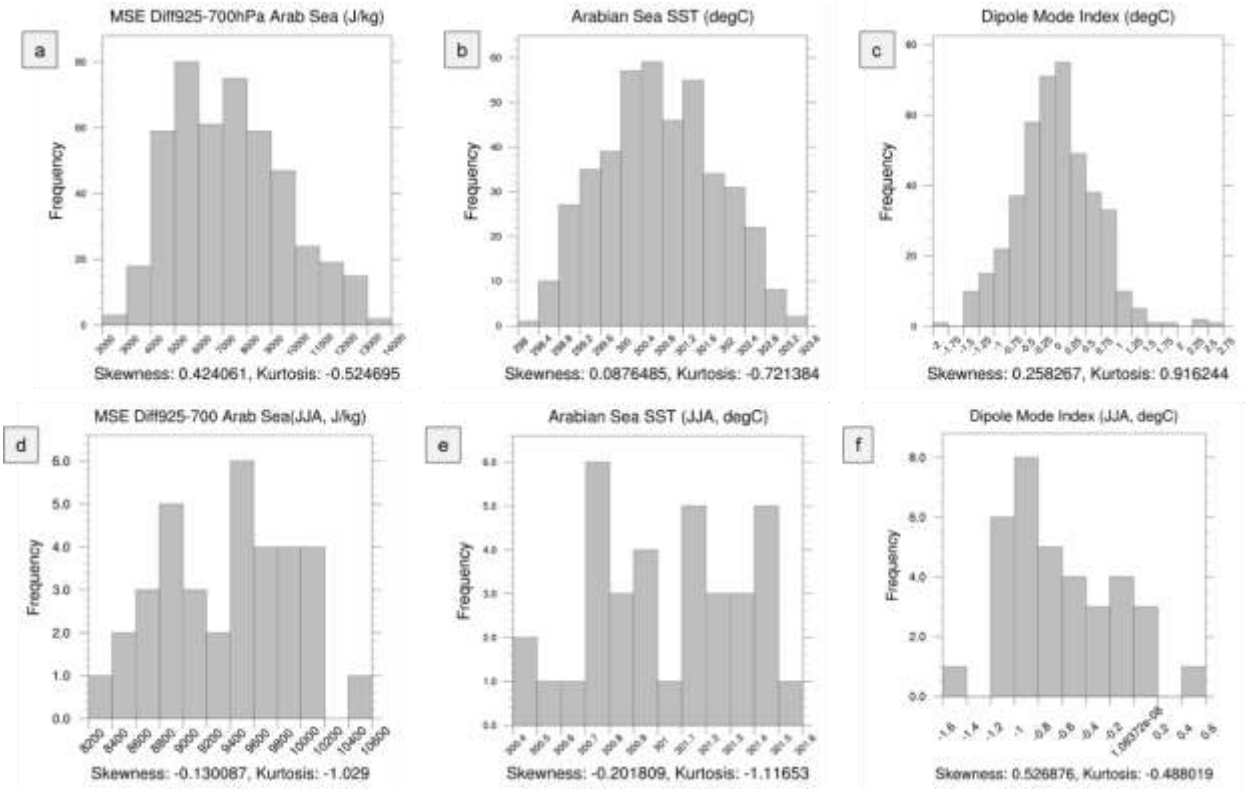

Figure 19: Three indices that were not bimodal in the distributions of their monthly values (a-c) but were bimodal in their JJA values (d-f)

6.2.3. Correlations between Indices

As expected, correlation values between the indices and especially between solar radiation and the various monsoon indices dropped off sharply with the consideration of only JJA values (Table A4). It should be noted that the correlation of any variable with the solar radiation – being constant across the years in this case – has no physical significance or relevance whatsoever. We also observe more correlations coming out where previously there were none (such as between monsoon indices and ENSO indices, and between monsoon indices and the DMI index). A condensed version of this table is given in Table 2. We observe that the most correlations occurring between monsoon and ENSO indices. Two monsoon indices – the zonal vertical shear ("vert_shear_u") and velocity potential at 850hPa ("vp850") – correlate strongly (>0.4) with three of the five ENSO indices. Four other monsoon indices – moisture flux over India ("MF_Ind"), moist static energy index over the Arabian Sea ("MSE_Arab"), Arabian Sea surface temperatures ("Arab_temp"), and the land-sea temperature gradient ("LSTG") – correlate with one or two ENSO indices, and exclusive the SOI and ESOI indices. Two interesting observations may be made here. First, the monsoon variables correlated with more ENSO indices tend to be dynamical in nature (vertical wind shear and velocity potential), while those monsoon indices only correlated with one or two ENSO indices are thermodynamic (moisture flux, moist static energy, etc.). Second, these thermodynamic monsoon variables are exclusively correlated with pressure-based ENSO indices (SOI and ESOI), while the dynamical monsoon variables are correlated with both pressure-based and sea surface temperature-based (Niño3.4-SST and ONI) ENSO indices. To summarize, the strongest and greatest number of correlations between ENSO and the monsoon are manifested in not in the rainfall but in dynamical variables of the monsoon and, among the ENSO indices, pressure-based indices capture more correlation than SST-based indices. Even more specifically, the ESOI index correlates with more monsoon indices (5) than does the SOI index (only 2). Therefore, a possible conclusion to be had from these results is that if in past studies little correlation has been found between the monsoon and ENSO, perhaps this

Table 2 – Correlations between monsoon indices (top) and indices of ENSO (orange), warming (red), and the IOD (purple) (left).

	solar_rad	precip_EIMR	vert_shear_u	vp200	vp850	rhavg400700	MF_Ind	MF_Arab	MSE_Ind	MSE_Arab	Ind_temp	Arab_temp	LSTG
Nino3.4-SST	0.168	0.209	0.422	-0.109	0.476	-0.285	0.312	-0.114	-0.017	0.346	-0.057	0.278	-0.351
ONI	0.168	0.212	0.437	-0.113	0.480	-0.286	0.298	-0.118	-0.029	0.352	-0.056	0.296	-0.364
SOI	-0.186	-0.246	-0.250	-0.040	-0.339	0.329	-0.415	-0.084	0.097	-0.366	0.194	-0.215	0.440
ESOI	-0.222	-0.286	-0.479	0.120	-0.502	0.188	-0.241	0.151	0.121	-0.416	0.136	-0.417	0.541
eq_OLR	0.157	0.086	0.397	-0.067	0.364	-0.304	0.190	-0.018	0.120	0.246	0.168	0.328	-0.150
glob_temp_a	-0.108	-0.401	0.114	-0.335	0.040	-0.205	-0.071	-0.199	0.737	0.099	0.695	0.219	0.503
glob_SST_an	-0.135	-0.215	0.298	-0.379	0.239	-0.125	-0.101	-0.219	0.669	0.180	0.605	0.368	0.288
DMI	0.319	0.368	0.160	0.218	0.473	-0.040	0.278	0.188	0.010	0.159	-0.131	0.297	-0.450

can be attributed to the use of "traditional" monsoon and ENSO indices such as total rainfall and SOI or an SST-based index. What these results show is the strength of the ESOI index and of "alternative" monsoon indices such as velocity potential and vertical wind shear at capturing correlations between these two processes. We speculate that, since SOI appears to be a weaker index to capture correlation between the monsoon and ENSO, perhaps the influence of ENSO on the monsoon is manifested in some perturbation of atmospheric circulation at the equator, since this is where ESOI is measured. This assumes that our procedure has accounted for all confounding factors between the different indices, of which we expect the seasonal cycle is likely the greatest and we believe we have accounted for by considering only JJA values of the indices.

When considering the other two processes postulated to influence the monsoon – global warming and the IOD – we observe many fewer instances of correlation, with the warming indices only correlating strongly (>0.4) with three monsoon indices total and the DMI index only correlating strongly with one. The warming indices do have very high correlations with India land surface temperature (>0.6) and the moist static energy index over India (>0.7). This high correlation might be a factor of the relatively quick response time of the land surface warming as compared to the ocean, which has a much higher heat capacity and thermal inertia. We don't attribute any obvious effect of global warming on the monsoon on the basis of this data, although it suggests that perhaps the most important effect of global warming on the monsoon will be in dynamics related to the land temperature and associated instability and convection (as parameterized by moist static energy). Compared to the correlations between the monsoon and ENSO, however, these weak patterns and correlations force us to conclude that the data is inconclusive on the question of global warming's and the IOD's influence on the monsoon.

7. Conclusions

The important findings from each section of the statistical results have been extracted and discussed in terms of their interpretation and significance here. The most significant findings are denoted by asterisks.

5. Time Series of the Indices

(1) Monthly time series of the indices accurately capture the seasonal fluctuation of monsoon variables as well as the historical record of global warming and observed ENSO and IOD events. The time series of JJA values of the indices illustrate the elimination of the

effect of the seasonal cycle on the indices by removing the fluctuations seen in the monsoon indices and by displaying a virtually-constant value of incoming solar radiation, the primary seasonal forcing of many of these indices. The time series plots in this section have served both to illustrate that removal of the seasonal signal in the JJA values, as well as to demonstrate the robustness of the indices in capturing basic, well-understood patterns associated with these phenomena.

6.1 Monthly Values (The Seasonal Cycle)

(2) *6.1.1.* Normality of the Indices' Distributions: The distributions of monthly values in the indices tend towards non-normal distributions, specifically negative (flatter-distribution) kurtosis values and positive (right-tailed) skewness values. The flatness of the distributions is attributed to the seasonal cycle experienced by most of the indices. The range of values produced by such strong seasonal fluctuations as those experienced by monsoon indices (and to a lesser but still considerable extent, the ENSO and IOD indices) results in this flatter-than-normal distribution. The strong skew of some indices is attributed to the values in the three "extreme" monsoon months of the year dragging the distribution away from the mean values of the other nine months of the year; bimodality in the distributions (related to the seasonal cycle) was also occasionally responsible for high values of skew. We hypothesized that skewness and kurtosis would both be reduced in considering only JJA values, reducing the bimodal and/or skewing effect of the seasonal cycle. Skewness was found to be reduced in the distributions of JJA values, but kurtosis was not (section 6.2.1).

(3) *6.1.2* Bimodality of the Indices: The vast majority of monsoon indices exhibit bimodality in their distributions of monthly values due to the strong seasonality of these indices. Correspondingly, ENSO, warming, and IOD indices did not exhibit such strong values of bimodality. The strength of the seasonal signal in the monsoon indices caused the distributions of their monthly values to commonly be centered around two peaks, which we attributed to summer/monsoon-season and winter-season values of the various indices. All other indices exhibited weaker bimodality although not extremely low values thereof, indicating a perhaps slight influence of the seasonal cycle on them. This justifies our procedure of taking the JJA values of each index to account for and remove the confounding influence of this cycle. Finally, we predicted the bimodality of the indices to decrease with the removal of the seasonal cycle, and it did, although not completely (section 6.2.2).

(4) *6.1.3* Correlations between Indices: Correlations between monthly values of the indices are overwhelmed by the seasonal signal, with very high correlation values (>0.6) between solar radiation and the majority of the monsoon indices. We also observed no significant correlation between the monsoon and ENSO, warming, or the IOD at this monthly frequency. This simply demonstrates the strong influence of the seasonal cycle on the monsoon variables, although it is less overpowering of ENSO and the IOD, which are more interannual phenomena than seasonal. There was a constant pattern of high correlation with the global land surface temperature anomaly with all but one of the monsoon indices; the reason for this could not be determined but the values are high enough to suspect some mistake or miscalculation appearing in the code (the code could not be successfully debugged at the time of submission of this thesis). We hypothesized that this strong tracking of monsoon indices and solar radiation would be greatly reduced among JJA values, and it was (discussed in section 6.2.3), allowing other trends and correlations to be revealed.

6.2 JJA Values (Interannual Variation)

(5) *6.2.1.* Normality of the Indices' Distributions: These distributions retained the negative kurtosis values observed in the distributions of monthly index values but showed greatly reduced skewness. We attributed the reduced skewness (enhanced symmetry) to the elimination of the seasonal cycle, which would either give bimodal distributions centered at two summer- and winter-based values or give skew by the three "extreme" monsoon months dragging out the mean values of the other nine months of the year. The retention of high negative kurtosis (indicative of flatter-than-normal distributions) suggests that, even after having limited the data to a single season, there is still a decent enough spread in the indices to have their distributions deviate from normality in this way.

*****(6) *6.2.2.* Bimodality of the Indices: The bimodality of the indices was reduced in virtually all cases by having removed the effect of the seasonal cycle; however this reduce was only slight and bimodality was not eliminated completely from any of the indices.** This is a significant finding of this study as it is evidence of a possible inherent bimodality to some of the indices, especially the monsoon indices which exhibited bimodality more commonly than did the ENSO indices. The irony in this is that ENSO is most commonly understood (arguably erroneously) as a manifestation of two distinct states – El Niño versus La Niña conditions – even though it is more accurately understood as a unimodal rather than bimodal range of conditions that occasionally qualify as El Niño or La Niña. Conversely, the monsoon, which is not currently

understood to exist as a bimodal system, exhibits the most considerable bimodality in this analysis. Having eliminated the effect of its bimodal forcing (by assessing only JJA values), we attribute this residual bimodality to the internal dynamics of the monsoon itself; we postulate that if the bimodality is not external and attributable to a bimodal forcing, then it must be internal and inherent to the system itself. There is a limited body of work on different oscillation periods manifesting in the monsoon (Narasimha and Kailas (2001) and Narasimha and Bhattacharyya (2010), but these oscillations are based on rainfall data, which is not one of the indices we observe to exhibit bimodality here. These results present an intriguing possibility of inherent bimodality to the monsoon that warrants further investigation.

*****(6) *6.2.3.* Correlations between Indices: Correlations between solar radiation (which is now essentially constant) and monsoon indices drop off considerably, revealing correlations between monsoon indices and other indices, mainly those of ENSO. Such correlations are better captured by dynamical monsoon indices than thermodynamic monsoon indices and by pressure-based ENSO indices (especially ESOI) rather than SST-based ENSO indices.** These findings present a unique pattern of correlation between ENSO and the monsoon that, with some speculation, may inform how the two climate phenomena are connected. Given ESOI's strong correlation with a high number of monsoon indices (5), we postulate that the most likely connection between the monsoon and ENSO might be manifested through atmospheric circulations over the equator, where the ESOI is measured. We additionally advise future studies to consider the use of "alternative" monsoon indices such as vertical wind shear and velocity potential at 850hPa over more traditional indices such as total rainfall, which was not found to correlate with any ENSO indices. Finally, correlations between the monsoon and global warming and the IOD were sparse and weak; the ENSO indices presented much more correlation.

In conclusion, this study has made a through and systematic study of the statistical features of climate indices measuring the Indian monsoon, ENSO, global warming, and the IOD in an attempt to illuminate connections between these phenomena. The most profound findings of this study are as follows. Firstly, unique correlation patterns between ENSO and the monsoon are revealed in JJA values of their respective indices, and evidence was found of dynamical monsoon indices and pressure-based ENSO indices being more highly correlated than other types of indices. There was no such pattern of significant correlation with global warming or the IOD. Secondly, an interesting retention of bimodality was observed in many of the indices, even after having removed the bimodal external forcing of them (namely the seasonal cycle). We

therefore tentatively attribute the weak but not negligible bimodality of these indices to some bimodal tendency inherent to their own dynamics; whatever bimodality is not attributable to external forcing must be an internal feature of the monsoon, and we project this finding as new and interesting evidence of oscillations in the monsoon that warrants further investigation. The significance of this study, then, is evidence of the statistical relevance of certain monsoon and ENSO indices over others and of a new and interesting bimodality that is perhaps present in the monsoon system, as evinced by a number of its indices.

While such a study as this cannot inform any mechanisms or causation for these observations, it does offer some quantitative, statistically-founded analysis on which future studies might be based. It represents an important first step towards characterizing these complex climatic processes, having investigated their most basic variables in a compartmentalized and systematic manner. If nothing else, we believe the significance of this study lies in these findings illuminating new possibilities of connections between the monsoon and various climate phenomena (particularly ENSO), thus informing new unconsidered directions of future study on these questions.

8. Acknowledgements

I'd like to acknowledge Dr. Ronald B. Smith, Professor of Geology and Geophysics at Yale University, and of Dr. Caroline C. Ummenhofer, Associate Scientist at Woods Hole Oceanographic Institution, for their mentorship and guidance in this project. The reanalysis data set for this project was provided by the NOAA/OAR/ESRL PSD, Boulder, Colorado, USA, from their web site at https://www.esrl.noaa.gov/psd/.

9. References

Allan, R. P., & Soden, B. J. (2008). Atmospheric warming and the amplification of precipitation extremes. *Science*, *321*(5895), 1481-1484.

Anil, N., Kumar, M. R., Sajeev, R., & Saji, P. K. (2016). Role of distinct flavours of IOD events on Indian summer monsoon. *Natural Hazards*, *82*(2), 1317-1326.

Barnston, A. (2015, January 29). *Why are there so many ENSO indexes, instead of just one?* NOAA Climate.gov. Retrieved from https://www.climate.gov/news-features/blogs/enso/why-are-there-so-many-enso-indexes-instead-just-one.

Basha, G., Kishore, P., Ratnam, M. V., Jayaraman, A., Kouchak, A. A., Ouarda, T. B., & Velicogna, I. (2017). Historical and Projected Surface Temperature over India during the 20 th and 21 st century. *Scientific reports*, *7*(1), 2987.

Dahlman, L. (2009, August 30). *Climate Variability: Oceanic Niño Index*. NOAA Climate.gov. Retrieved from https://www.climate.gov/news-features/understanding-climate/climate-variability-oceanic-ni%C3%B1o-index.

"Dipole Mode Index (DMI)". NOAA Ocean Observations Panel for Climate. Retrieved from https://stateofthe ocean.osmc.noaa.gov/sur/ind/dmi.php.

"Extended Reconstructed Sea Surface Temperature (ERSST)". NOAA National Centers for Environmental Information. Retrieved from https://www.ncdc.noaa.gov/data-access/marineocean-data/extended-reconstructed-sea-surface-temperature-ersst.

Forootan, E., Awange, J. L., Schumacher, M., Anyah, R. O., van Dijk, A. I. J. M., & Kusche, J. (2016). Quantifying the impacts of ENSO and IOD on rain gauge and remotely sensed precipitation products over Australia. *Remote sensing of Environment*, *172*, 50-66.

"GISS Surface Temperature Analysis". NASA Goddard Institute for Space Studies. Retrieved from https://data. giss.nasa.gov/gistemp/graphs_v3/.

Goswami, B. N., Sengupta, D., & Kumar, G. S. (1998). Intraseasonal oscillations and interannual variability of surface winds over the Indian monsoon region. *Proceedings of the Indian Academy of Sciences-Earth and Planetary Sciences*, *107*(1), 45-64.

Goswami, B. N., Krishnamurthy, V., & Annmalai, H. (1999). A broad-scale circulation index for the interannual variability of the Indian summer monsoon. *Quarterly Journal of the Royal Meteorological Society*, *125*(554), 611-633.

Goswami, B. N., & Mohan, R. A. (2001). Intraseasonal oscillations and interannual variability of the Indian summer monsoon. *Journal of Climate*, *14*(6), 1180-1198.

Goswami, B. N., Chakravorty, S. (2017). Dynamics of the Indian Summer Monsoon climate. In *Oxford Research Encyclopedia of Climate Science*. Retrieved from http://climatescience.oxfordre.com/view/10.1093/acrefore/ 9780190228620.001.0001/acrefore-9780190228620-e-613.

Hansen, J., Ruedy, R., Sato, M., & Lo, K. (2010). Global surface temperature change. *Reviews of Geophysics*, *48*(4).

Kalnay, E., Kanamitsu, M., Kistler, R., Collins, W., Deaven, D., Gandin, L., ... & Zhu, Y. (1996). The NCEP/NCAR 40-year reanalysis project. *Bulletin of the American meteorological Society*, *77*(3), 437-471.

Kanamitsu, M., Ebisuzaki, W., Woollen, J., Yang, S. K., Hnilo, J. J., Fiorino, M., & Potter, G. L. (2002). Ncep–doe amip-ii reanalysis (r-2). *Bulletin of the American Meteorological Society*, *83*(11), 1631-1643.

Krishnamurthy, V., & Goswami, B. N. (2000). Indian monsoon–ENSO relationship on interdecadal timescale. *Journal of Climate*, *13*(3), 579-595.

Krishnamurthy, V., & Shukla, J. (2000). Intraseasonal and interannual variability of rainfall over India. *Journal of Climate*, *13*(24), 4366-4377.

Kumar, K. K., Rajagopalan, B., & Cane, M. A. (1999). On the weakening relationship between the Indian monsoon and ENSO. *Science*, *284*(5423), 2156-2159.

Li, Z., Chao, Y., & McWilliams, J. C. (2006). Computation of the streamfunction and velocity potential for limited and irregular domains. *Monthly weather review*, *134*(11), 3384-3394.

Moist Static Energy [Def. 1]. In *American Meteorology Society Glossary of Meteorology*, Retrieved March 18, 2018, from http://glossary.ametsoc.org/wiki/Moist_static_energy.

Narasimha, R., & Kailas, S. V. (2001). A wavelet map of monsoon variability. *PROCEEDINGS-INDIAN NATIONAL SCIENCE ACADEMY PART A*, *67*(3), 327-342.

Narasimha, R., & Bhattacharyya, S. (2010). A wavelet cross-spectral analysis of solar–ENSO–rainfall connections in the Indian monsoons. *Applied and Computational Harmonic Analysis*, *28*(3), 285-295.

The NCAR Command Language (Version 6.4.0) [Software]. (2017). Boulder, Colorado: UCAR/NCAR/CISL/TDD. http://dx.doi.org/10.5065/D6WD3XH5.

Niño SST Indices. (2018). NCAR UCAR Climate Data Guide. Retrieved from https://climatedataguide.ucar.edu/ climate-data/nino-sst-indices-nino-12-3-34-4-oni-and-tni.

"Outgoing Longwave Radiation (OLR), NOAA National Centers for Environmental Information. Retrieved from https://www.ncdc.noaa.gov/teleconnections/enso/indicators/olr/.

"Outoing Longwave Radiation (OLR)". (2002). NOAA Climate Prediction Center. Retrieved from http://www.cpc.ncep.noaa.gov/products/global_precip/html/wpage.olr.html.

Parker, D. J., Willetts, P., Birch, C., Turner, A. G., Marsham, J. H., Taylor, C. M., ... & Martin, G. M. (2016). The interaction of moist convection and mid-level dry air in the advance of the onset of the Indian monsoon. *Quarterly Journal of the Royal Meteorological Society*, *142*(699), 2256-2272.

Parthasarathy, B., Kumar, K. R., & Kothawale, D. R. (1992). Indian summer monsoon rainfall indices: 1871-1990. *Meteorological Magazine*, *121*(1441), 174-186.

Rasmusson, E. M., & Carpenter, T. H. (1982). Variations in tropical sea surface temperature and surface wind fields associated with the Southern Oscillation/El Niño. *Monthly Weather Review*, *110*(5), 354-384.

Rasmusson, E. M., & Wallace, J. M. (1983). Meteorological aspects of the El Nino/southern oscillation. *Science*, *222*(4629), 1195-1202.

Roxy, M. K., Ritika, K., Terray, P., & Masson, S. (2014). The curious case of Indian Ocean warming. *Journal of Climate*, *27*(22), 8501-8509.

Saji, N. H., Goswami, B. N., Vinayachandran, P. N., & Yamagata, T. (1999). A dipole mode in the tropical Indian Ocean. *Nature*, *401*(6751), 360.

Shukla, J., & Mooley, D. A. (1987). Empirical prediction of the summer monsoon rainfall over India. *Monthly Weather Review*, *115*(3), 695-704.

"Status of IOD". Indian National Centre for Ocean Information Services. Retrieved from http://www.incois.gov. in/portal/IOD.

"Southern Oscillation Index (SOI) and Equatorial SOI". International Research Institute for Climate and Society, Columbia University. Retrieved from https://iridl.ldeo.columbia.edu/maproom/ENSO/Time_Series/Equatorial _SOI.html

Thermal Wind Equation [Def. 1]. In *American Meteorology Society Glossary of Meteorology*, Retrieved March 15, 2018, from http://glossary.ametsoc.org/wiki/Thermal_wind_equation.

Torrence, C., & Webster, P. J. (1999). Interdecadal changes in the ENSO–monsoon system. *Journal of Climate*, *12*(8), 2679-2690.

Trenberth, K. E. (1997). The definition of el nino. *Bulletin of the American Meteorological Society*, *78*(12), 2771-2777.

Trenberth, K. E., & Stepaniak, D. P. (2001). Indices of el niño evolution. *Journal of climate*, *14*(8), 1697-1701.

Troup, A. J. (1965). The 'southern oscillation'. *Quarterly Journal of the Royal Meteorological Society*, *91*(390), 490-506.

Velocity Potential [Def. 1]. In *American Meteorology Society Glossary of Meteorology*, Retrieved March 15, 2018, from http://glossary.ametsoc.org/wiki/Velocity_potential.

Webster, P. J., & Yang, S. (1992). Monsoon and ENSO: Selectively interactive systems. *Quarterly Journal of the Royal Meteorological Society*, *118*(507), 877-926.

Wentz, F. J., Ricciardulli, L., Hilburn, K., & Mears, C. (2007). How much more rain will global warming bring?. *Science*, *317*(5835), 233-235.

APPENDIX

A1. Statistical Methods

Skewness and Kurtosis

Skewness and kurtosis values were calculated with the NCL function "dim_stat4". This function computes the first four moments (average, sample variance, skewness, and kurtosis) of a vector

of values. Skewness is a measure of departure from symmetry (a normal distribution will be perfectly symmetrical and thus have no skew), while kurtosis is a measure of the spread (peak or flatness) of a distribution. The formulas for skewness and kurtosis that are used in the "dim_stat4" function are not given in NCL's documentation, but the documentation reports that a positive skewness indicates a tail trailing off to the right of the distribution, while a negative skewness indicates a tail trailing off to the left. A skewness of zero indicates perfect symmetry. The kurtosis values produced by the "dim_stat4" function are "excess kurtosis" values – a deviation from the normal kurtosis value of three (excess kurtosis = absolute kurtosis value - 3). A positive excess kurtosis indicates a distribution more sharply peaked than a normal distribution, while a negative excess kurtosis indicates a flatter distribution than normal.

Bimodality

Bimodality was calculated from skewness and kurtosis values using Sarle's bimodality coefficient (Bimodality 1, or β) and the formula for bimodality for a finite sample (Bimodality 2, or b). The formulas for these values are given below, where γ is skewness, κ is absolute kurtosis, and n is the sample size.

$$\beta = \frac{\gamma^2 + 1}{\kappa}$$

$$b = \frac{\gamma^2 + 1}{\kappa + \frac{3(n-1)^2}{(n-2)(n-3)}}$$

The logic behind both of these formulations is that a bimodal distribution will either have a flatter distribution than normal (so a low kurtosis value), high asymmetry (high skewness value), or both – any of which would increase these coefficients. The threshold for designating a bimodal distribution is 0.5 for Sarle's bimodality coefficient (β) and 5/9 (or 0.555) for finite-sample bimodality (b).

Correlation coefficients

Correlation coefficients were calculated in Excel using the CORREL function. This function provides the Pearson Correlation Coefficient between two samples (the CORREL and PEARSON functions in Excel both use the same formula) which is given by:

$$r = \frac{\sum[(x - \bar{x})(y - \bar{y})]}{\sqrt{\sum(x - \bar{x})^2 \sum(y - \bar{y})^2}}$$

The Pearson correlation coefficient is a measure of the strength of a linear association between two variables, where a value of r = 1 indicates a perfect positive correlation and a value of r = -1 indicates a perfect negative correlation. This coefficient is limited in that it cannot inform the strength of non-linear relationships, but it is an intuitive and familiar statistic to present for the objective of this study, which is to investigate relationships between the monsoon and other climate phenomenon.

A2. Statistical Tables – Skewness, Kurtosis, and Bimodality, and Correlation Coefficients

Table A1 – Statistical Data of the Monthly Values of the Indices

All months	Mean	Std. Dev.	Skewness	(Excess) Kurtosis	Bimodality 1 (>0.5)	Bimodality 2 (>5/9)
solar_rad	386.841	62.172	-0.360	-1.400	0.706	0.607
precip_EIMR	151.157	123.840	0.637	-0.980	0.696	0.617
vert_shear_u	11.712	16.592	-0.371	-1.360	0.693	0.599
vp200	594123.967	1761246.391	0.197	-0.584	0.430	0.388
vp850	-261526.931	516651.353	0.519	0.224	0.394	0.364
rhavg400700	37.385	9.606	0.630	-0.802	0.636	0.568
MF_Ind	8.232	9.230	0.623	-0.920	0.667	0.593
MF_Arab	8.472	15.713	0.733	-0.978	0.761	0.674
MSE_Ind	6143.509	3722.694	0.038	-1.463	0.652	0.558
MSE_Arab	7287.453	2352.435	0.424	-0.525	0.477	0.431
Ind_temp	294.037	16.761	-0.313	-1.402	0.687	0.591
Arab_temp	300.734	1.174	0.090	-0.715	0.441	0.396
LSTG	-6.680198	11.6043	-0.24274	-1.449698	0.683	0.585
nino_34	0.002	1.080	-0.087	-0.436	0.393	0.357
ONI	27.083	1.035	-0.072	-0.375	0.383	0.348
SOI	551.455	219.158	0.375	-0.145	0.400	0.366
ESOI	0.015	1.016	-0.536	0.349	0.384	0.357
eq_OLR	472.022	4.344	-0.696	0.078	0.482	0.445
glob_temp_anom	0.024	1.712	0.307	-1.248	0.625	0.544
glob_SST_anom	0.004	0.126	0.283	0.067	0.352	0.325
DMI	0.000	0.645	0.258	0.916	0.272	0.255

Table A2 – Statistical Data of the Annual JJA-average Values of the Indices

JJA	Mean	Std. Dev.	Skewness	(Excess) Kurtosis	Bimodality 1 (>0.5)	Bimodality 2 (>5/9)
solar_rad	450.584	0.106	0.012	-1.254	0.573	0.499
precip_EIMR	332.816	22.680	0.097	-0.534	0.409	0.370
vert_shear_u	-11.342	1.502	0.013	-0.893	0.475	0.423
vp200	-1045281.711	599686.927	0.148	-0.419	0.396	0.360
vp850	258475.167	281246.360	-0.134	-0.749	0.452	0.405
rhavg400700	51.397	2.079	-0.029	-0.435	0.390	0.354
MF_Ind	22.191	1.473	-0.341	-0.850	0.519	0.463
MF_Arab	32.862	1.812	-0.286	0.118	0.347	0.320
MSE_Ind	10742.973	545.570	-0.450	-0.042	0.407	0.374
MSE_Arab	9359.961	559.414	-0.130	-1.029	0.516	0.456
Ind_temp	298.266	0.130	0.053	-0.639	0.425	0.383
Arab_temp	301.036	0.096	-0.202	-1.117	0.553	0.486
LSTG	-2.760	0.125	-1.040	1.464	0.466	0.441
nino_34	0.198	0.756	0.251	-0.052	0.361	0.331
ONI	27.290	0.733	0.306	-0.069	0.373	0.343
SOI	402.857	126.401	-0.221	-0.541	0.427	0.386
ESOI	0.318	0.691	-0.778	0.293	0.488	0.452
eq_OLR	473.261	2.980	-0.309	-1.118	0.582	0.511
glob_temp_anom	0.035	0.400	-0.253	-1.060	0.549	0.484
glob_SST_anom	0.000	0.146	0.077	-0.593	0.418	0.377
DMI	-0.605	0.461	0.527	-0.488	0.509	0.461

Table A3 – Correlations Between Indices Monthly Values

	solar_rad	precip_EIMR	vert_shear_u	vp200	vp850	rhavg400700	MF_Ind	MF_Arab	MSE_Ind	MSE_Arab	Ind_temp	Arab_temp	LSTG	Nino3.4-SST	ONI	SOI	ESOI	eq_OLR	glob_temp_a	glob_SST_an	DMI
solar_rad	1.000																				
precip_EIMR	0.716	1.000																			
vert_shear_u	-0.753	-0.967	1.000																		
vp200	-0.490	-0.680	0.707	1.000																	
vp850	0.586	0.686	-0.608	-0.338	1.000																
rhavg400700	0.724	0.939	-0.927	-0.681	0.584	1.000															
MF_Ind	0.826	0.900	-0.879	-0.603	0.628	0.901	1.000														
MF_Arab	0.777	0.962	-0.939	-0.644	0.649	0.944	0.968	1.000													
MSE_Ind	0.825	0.913	-0.946	-0.705	0.629	0.884	0.856	0.893	1.000												
MSE_Arab	0.656	0.725	-0.730	-0.586	0.644	0.629	0.647	0.684	0.848	1.000											
Ind_temp	0.948	0.794	-0.842	-0.580	0.654	0.760	0.803	0.796	0.918	0.796	1.000										
Arab_temp	0.589	0.382	-0.391	-0.268	0.588	0.269	0.303	0.310	0.560	0.734	0.717	1.000									
LSTG	0.954	0.834	-0.888	-0.612	0.600	0.829	0.869	0.859	0.927	0.723	0.975	0.544	1.000								
Nino3.4-SST	0.346	0.107	-0.066	-0.040	0.295	0.117	0.222	0.138	0.211	0.244	0.316	0.395	0.255	1.000							
ONI	0.330	0.109	-0.065	-0.048	0.273	0.124	0.229	0.141	0.204	0.226	0.295	0.352	0.243	0.994	1.000						
SOI	-0.479	-0.433	0.403	0.274	-0.397	-0.418	-0.475	-0.435	-0.490	-0.445	-0.502	-0.420	-0.471	-0.727	-0.736	1.000					
ESOI	-0.024	0.278	-0.321	-0.239	0.088	0.217	0.082	0.204	0.217	0.218	0.111	0.065	0.113	-0.745	-0.768	0.500	1.000				
eq_OLR	0.119	0.219	-0.195	-0.201	0.242	0.200	0.170	0.178	0.274	0.291	0.214	0.280	0.169	0.704	0.716	-0.622	-0.382	1.000			
glob_temp_a	0.711	0.923	-0.929	-0.682	0.678	0.880	0.854	0.901	0.926	0.786	0.821	0.488	0.832	0.163	0.158	-0.443	0.300	0.301	1.000		
glob_SST_an	0.005	-0.004	0.039	-0.051	0.174	0.006	0.014	-0.007	0.074	0.097	0.049	0.146	0.013	0.263	0.268	-0.036	-0.112	0.312	0.196	1.000	
DMI	-0.109	-0.404	0.380	0.254	-0.147	-0.418	-0.434	-0.475	-0.251	-0.109	-0.098	0.289	-0.210	0.271	0.248	-0.043	-0.283	0.064	-0.368	0.056	1.000

Table A5 – Correlations Between Indices Amongst Only JJA Values

	solar_rad	precip_EIMR	vert_shear_u	vp200	vp850	rhavg400700	MF_Ind	MF_Arab	MSE_Ind	MSE_Arab	Ind_temp	Arab_temp	LSTG	Nino3.4-SST	ONI	SOI	ESOI	eq_OLR	glob_temp_a	glob_SST_an	DMI
solar_rad	1.000																				
precip_EIMR	0.189	1.000																			
vert_shear_u	0.226	-0.148	1.000																		
vp200	0.132	0.259	-0.290	1.000																	
vp850	0.115	0.476	0.248	-0.223	1.000																
rhavg400700	-0.059	0.488	-0.221	-0.087	0.275	1.000															
MF_Ind	0.021	0.330	-0.428	-0.123	0.305	-0.049	1.000														
MF_Arab	-0.099	0.546	-0.543	0.483	-0.039	0.259	0.353	1.000													
MSE_Ind	-0.182	-0.478	0.247	-0.209	-0.181	-0.506	-0.151	-0.250	1.000												
MSE_Arab	0.101	-0.348	0.506	-0.205	-0.093	-0.550	-0.075	-0.395	0.487	1.000											
Ind_temp	0.019	-0.585	0.383	-0.472	0.010	-0.427	-0.140	-0.560	0.683	0.422	1.000										
Arab_temp	0.344	-0.098	0.840	-0.199	0.224	-0.173	-0.314	-0.405	0.339	0.596	0.463	1.000									
LSTG	-0.303	-0.517	-0.355	-0.325	-0.210	-0.222	0.106	-0.243	0.388	-0.127	0.609	-0.413	1.000								
Nino3.4-SST	0.168	0.209	0.422	-0.109	0.476	-0.285	0.312	-0.114	-0.017	0.346	-0.057	0.278	-0.351	1.000							
ONI	0.168	0.212	0.437	-0.113	0.480	-0.286	0.298	-0.118	-0.029	0.352	-0.056	0.296	-0.364	0.998	1.000						
SOI	-0.186	-0.246	-0.250	-0.040	-0.339	0.329	-0.415	-0.084	0.097	-0.366	0.194	-0.215	0.440	-0.865	-0.866	1.000					
ESOI	-0.222	-0.286	-0.479	0.120	-0.502	0.188	-0.241	0.151	0.121	-0.416	0.136	-0.417	0.541	-0.873	-0.891	0.850	1.000				
eq_OLR	0.157	0.086	0.397	-0.067	0.364	-0.304	0.190	-0.018	0.120	0.246	0.168	0.328	-0.150	0.815	0.824	-0.700	-0.652	1.000			
glob_temp_a	-0.108	-0.401	0.114	-0.335	0.040	-0.205	-0.071	-0.199	0.737	0.099	0.695	0.219	0.503	-0.182	-0.192	0.374	0.303	0.017	1.000		
glob_SST_an	-0.135	-0.215	0.298	-0.379	0.239	-0.125	-0.101	-0.219	0.669	0.180	0.605	0.368	0.288	0.060	0.064	0.183	0.002	0.251	0.856	1.000	
DMI	0.319	0.368	0.160	0.218	0.473	-0.040	0.278	0.188	0.010	0.159	-0.131	0.297	-0.450	0.363	0.346	-0.464	-0.413	0.145	-0.080	-0.053	1.000